Biochimica et Biophysica Acta 1818 (2012) 384–401

Contents lists available at SciVerse ScienceDirect

Biochimica et Biophysica Acta

journal homepage: www.elsevier.com/locate/bbamem

Interaction of the full-length Bax protein with biomimetic mitochondrial liposomes: A small-angle neutron scattering and fluorescence study

Dmitri Satsoura [a], Norbert Kučerka [b], Sanjeevan Shivakumar [a], Jeremy Pencer [b], Corrie Griffiths [a], Brian Leber [a,c], David W. Andrews [a], John Katsaras [b,d], Cécile Fradin [a,e,*]

[a] Department of Biochemistry and Biomedical Sciences, McMaster University Health Sciences Centre, Hamilton, Ontario, Canada L8N 3Z5
[b] Canadian Neutron Beam Centre, National Research Council, Chalk River, Ontario, Canada K0J 1J0
[c] Department of Medicine, McMaster University Health Sciences Centre, Hamilton, Ontario, Canada L8N 3Z5
[d] Neutron Scattering Science Division, Oak Ridge National Laboratory, Oak Ridge, TN 37831-6475, USA
[e] Department of Physics and Astronomy, McMaster University, Hamilton, Ontario, Canada L8S 4M1

ARTICLE INFO

Article history:
Received 29 March 2011
Received in revised form 15 September 2011
Accepted 7 October 2011
Available online 15 October 2011

Keywords:
Apoptosis
Bcl-2 family protein
Bax
FCS
FIDA
SANS

ABSTRACT

In response to apoptotic stimuli, the pro-apoptotic protein Bax inserts in the outer mitochondrial membrane, resulting in the formation of pores and the release of several mitochondrial components, and sealing the cell's fate. To study the binding of Bax to membranes, we used an in vitro system consisting of 50 nm diameter liposomes prepared with a lipid composition mimicking that of mitochondrial membranes in which *recombinant* purified full-length Bax was inserted via activation with purified tBid. We detected the association of the protein with the membrane using fluorescence fluctuation methods, and found that it could well be described by an equilibrium between soluble and membrane-bound Bax and that at a high protein-to-liposome ratio the binding seemed to saturate at about 15 Bax proteins per 50 nm diameter liposome. We then obtained structural data for samples in this saturated binding regime using small-angle neutron scattering under different contrast matching conditions. Utilizing a simple model to fit the neutron data, we observed that a significant amount of the protein mass protrudes above the membrane, in contrast to the conjecture that all of the membrane-associated Bax states are umbrella-like. Upon protein binding, we also observed a thinning of the lipid bilayer accompanied by an increase in liposome radius, an effect reminiscent of the action of antimicrobial peptides on membranes.

1. Introduction

Apoptosis is a highly regulated type of programmed cell death essential to the development and maintenance of tissues and to the defense of organisms against pathogens [1]. Many of the known apoptotic pathways involve mitochondrial damage, where permeabilization of the outer mitochondrial membrane results in leakage of a number of apoptotic factors, including cytochrome c, into the cytoplasm [2]. This important step just upstream of caspase activation and cell death is regulated by the Bcl-2 family of proteins [3–5]. Pro-apoptotic members of this family act to promote the release of apoptotic factors from the mitochondrial intermembrane space, while anti-apoptotic members act to inhibit it. For a significant number of Bcl-2 family proteins, this function is mediated by a direct interaction with lipid membranes – some family members, such as Bcl-2, Bcl-w and CED-9 are constitutively bound to membranes, while others significantly bind to membranes only after an activation step, for example cleavage in the case of Bid, and interaction with cleaved Bid in the case of Bax.

Human Bax is a 22 kDa (192 amino acids) pro-apoptotic Bcl-2 family member of particular physiological relevance because it can form pores in mitochondrial membranes [6], and because these pores are thought to be the functional units that allow for cytochrome c to be released during apoptosis [7]. In growing cells, Bax is mainly found in the cytoplasm, but at the onset of apoptosis it migrates to the outer mitochondrial membrane [8,9] where it undergoes a conformational change [7] and assembles into oligomers [10,11]. These events coincide with cytochrome c release [7]. In addition, many in vitro studies have shown that Bax is able to permeabilize lipid membranes [6,12–16]. The pore-forming activity of full-length Bax can be realized using the C-terminal fragment of Bid (noted as tBid for truncated Bid), which causes soluble monomeric Bax to bind to lipid membranes and oligomerize [15–17].

Abbreviations: wtBax, wild-type Bax; tBid, truncated Bid; SANS, small-angle neutron scattering; PC, phosphatidylcholine; PE, phosphatidylethanolamine; PI, phosphatidylinositol; PS, phosphatidylserine; CL, cardiolipin; DOPS, dioleoyl phosphatidylserine; TOCL, tetraoleoyl cardiolipin; EGFP, enhanced green fluorescent protein; FIDA, fluorescence intensity distribution analysis; FCS, fluorescence correlation spectroscopy; SDD, sample-to-detector distance; FWHM, full-width-at-half-maximum; SLD, scattering length density.

* Corresponding author at: Department of Physics and Astronomy, McMaster University, 1280 Main St. W, Hamilton, Ontario, Canada L8S 4M1. Tel.: +1 905 525 9140x23181; fax: +1 905 546 1252.
E-mail address: fradin@physics.mcmaster.ca (C. Fradin).

0005-2736/$ – see front matter © 2011 Elsevier B.V. All rights reserved.
doi:10.1016/j.bbamem.2011.10.007

The insertion of Bax into a membrane results in increased membrane conductivity [18], as well as the release of varying size particles [12,15,19,20] due to the formation of lipidic pores [16,21,22]. In contrast, anti-apoptotic Bcl-2 family members interacting with membranes (e.g. Bcl-2, Bcl-xL, Bcl-w, CED-9) do not seem to form pores – at least not large enough to allow for the release of particles such as cytochrome c. Instead they are thought to influence apoptosis through protein–protein interactions [3,5,23].

The soluble form structures of several Bcl-2 family proteins, including family members which are usually associated with membranes but become soluble when truncated, have been solved, e.g. Bcl-xL [24], Bcl-2 [25], Bcl-w [26], Bax [27], Bid [28,29] and CED-9 [30]. Interestingly, they all have a three-dimensional structure that is highly homologous to the soluble form of pore-forming bacterial colicins, and of diphtheria toxin, with a mainly hydrophobic α-helical hairpin (also containing charged residues) buried amongst six or seven amphipathic α-helices [31]. The structural homology displayed by these Bcl-2 family proteins, in their soluble form, is intriguing given the fact that they have diverging functions, namely anti-apoptotic (i.e. Bcl-xL, Bcl-2, Bcl-w, CED-9) or pro-apoptotic (i.e. Bax, Bid). However, the active membrane associated conformation of these proteins is still not well defined. In particular, the conformation(s) adopted by Bax when bound to a membrane is (or are) still unknown.

Even so, there are a few clues available regarding the membrane conformation(s) of Bax. Firstly, Bax can presumably adopt at least two conformations when binding to membranes. The clearest evidence of this is that in healthy cells a small fraction of Bax is found associated with mitochondria but remains carbonate extractable – corresponding to an inactive loosely-bound form of Bax, while in apoptotic cells Bax bound to mitochondrial membranes is no longer carbonate extractable – corresponding to a pore-forming membrane-inserted form of Bax [10,32]. Secondly, it is likely that the α-helical secondary structure of the monomeric soluble protein is conserved when the protein interacts with lipid membranes [17,33]. Thirdly, the Bax C-terminus (helix 9) has been identified as a transmembrane domain, while in vitro studies of single-point Bax mutants [34–36] and peptide studies [37,38] have implicated helices 5 and 6 in the formation of pores. It was later confirmed – by chemical labeling of single cysteine Bax mutants – that all three helices indeed insert in the outer mitochondrial membrane of apoptotic cells [39]. Finally, the Bax N-terminus (including helix 1), which interacts with tBid [7,32,34,35] and contains an epitope (6A7) that becomes accessible only after activation [40], has been shown to interact with lipid membranes [41,42] and is involved in mitochondrial targeting [34,36]. In conclusion, while helices 1, 5, 6 and 9 should be in contact with the membrane in membrane inserted pore-forming Bax, the configuration adopted by the remaining five helices is unknown. Moreover, the conformation(s) adopted by additional membrane bound forms of Bax, in particular by its predicted loosely-bound form, are unknown. Fig. 1 illustrates two possible pathways in which soluble Bax may insert in the membrane. We refer to Bax as being "inserted" in the membrane if one or several of its helices are transmembrane (e.g. conformations C and E in Fig. 1), and as being "peripherally bound" if interacting with the membrane without any transmembrane helices (e.g. conformations B and D in Fig. 1). Both "inserted" and "peripherally bound" Bax are collectively referred to as either being "bound" or "targeted" to the membrane.

Small-angle neutron scattering (SANS) has proven an ideal technique for studying the structure of liposomal membranes [43]. It is also a very promising technique for studying the conformation and quaternary structure of proteins in membranes, as it allows for the detection of large protein assemblies through the use of contrast variation experiments [43,44]. For example, SANS has been successfully used to study membrane oligomers formed by bacteriorhodopsin [44], SecA [45], and pneumolysin [46]. For this study, we have used a model system consisting of full-length recombinant Bax bound to the membranes

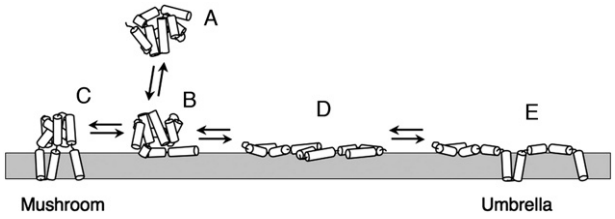

Fig. 1. Schematic representation of two possible pathways for the insertion of Bax into a lipid membrane. The soluble Bax protein (A) is thought to first peripherally associate with the membrane, or with proteins (i.e. tBid or Bax) already inserted in the membrane (B). The peripherally associated Bax protein may then insert into the membrane as follows: (i) it may insert helices 5, 6 and 9 in the lipid bilayer while retaining a globular conformation above the membrane (mushroom conformation, C); (ii) it may adopt an open conformation with all helices roughly parallel to the membrane (D) before inserting helices 5, 6 and 9 in the lipid bilayer (umbrella conformation, E). Interactions with tBid and other Bax molecules, both known to influence the insertion of Bax into the membrane, are not represented here.

of 50 nm diameter liposomes with a composition approximating that of mitochondrial membranes, and we have carried contrast variation SANS experiments to obtain information both on the conformation of Bax when bound to membranes and on the changes in the membrane caused by the binding of the protein. To complement the SANS experiments and support our choice of using small liposomes (made so that higher lipid concentrations and increased signal-to-noise levels could be achieved), we have carried out complementary fluorescence experiments in order to quantify the membrane binding and pore-formation activity of Bax in our model system.

2. Materials and methods

2.1. Liposome preparation

Liposomes were prepared from a mixture of lipids that reflects the overall lipid composition of *Xenopus* mitochondrial membranes, and which has been shown to support pore formation by tBid-activated Bax [15,17], i.e. phosphatidylcholine (PC), phosphatidylethanolamine (PE), phosphatidylinositol (PI), phosphatidylserine (PS) and cardiolipin (CL), with a mass ratio of 48:28:10:10:4. All lipids were purchased from Avanti Polar Lipids (Alabaster, AL, USA) either as purified from egg (PC, PE) or bovine liver (PI), or as synthetic lipids in the case of dioleoyl PS (DOPS) and tetraoleoyl CL (TOCL). The lipids were dissolved in chloroform and then mixed in the appropriate mass ratio. For fluorescence fluctuation experiments 0.008% by mass of the fluorescent dye DiD (Invitrogen Canada, Burlington, Canada) dissolved in methanol was added to the lipids. Solvents were then removed by evaporation under a stream of nitrogen gas, followed by incubation under vacuum for 2 h. Dry lipid films were resuspended in assay buffer (10 mM HEPES at pH 7, 200 mM KCl, 5 mM $MgCl_2$, 0.2 mM EDTA) to a total lipid concentration that varied from 0.5 to 40 g/l. The lipid solutions were then subjected to 10 freeze–thaw cycles and extruded through the pores of a Nucleopore track-etched polycarbonate membrane (Nucleopore, San Diego, CA, USA). Mostly, membranes with 50 nm pores were used, except for a few experiments when membranes with larger pores (100 nm or 200 nm) were used. Although the extruded liposomes are not strictly speaking monodisperse, they do follow a monomodal size distribution with a narrow polydispersity that effectively constitute a homogeneous sample (i.e. spherical unilamellar liposomes). The assay buffer was prepared with the appropriate fraction of H_2O and D_2O (Cambridge Isotopes, Andover, MA). HEPES was from BioShop Canada Inc (Burlington, Ontario, Canada), while all other chemicals were purchased from Sigma-Aldrich (Oakville, Ontario, Canada). Estimates for lipid concentrations were obtained by assuming that dry lipid films had been completely resuspended, that the extrusion step had no effect on lipid concentration, and that the average molecular weight of the phospholipids was 770 g/mol [47]. Estimates for

liposome concentrations were in turn obtained assuming that the lipids formed unilamellar liposomes with diameter 2R = 50 nm (or 100 nm or 200 nm), and that each phospholipid, on average, occupied a surface area of 0.75 nm^2 [48] (i.e. m ≈ 21,000 lipids per 50 nm diameter liposome). In some cases liposome concentrations were also directly measured by fluorescence as explained in Section 2.5.3.

2.2. Protein purification

Recombinant Bax and the C-terminal fragment of cleaved Bid (tBid) were obtained according to published protocols [27,49]. For both proteins great care was taken to remove all detergent molecules at the end of the purification process. Briefly, recombinant full-length human Bax (referred to as wild-type Bax – wtBax – in the following) with no additional amino acid residues was expressed in *Escherichia coli* as an intein/chitin binding domain fusion and purified using a chitin affinity chromatography column (New England Biolabs Ltd., Pickering, Ontario, Canada). The release of Bax from the column was achieved by intein self cleavage triggered by the addition of a buffer solution containing 2-mercaptoethanol (100 mM) and the detergent 3-[(3-Cholamidopropyl)-dimethylammonio]-1-propanesulfonate (CHAPS, 0.2% w/v), followed by incubation for 48 h. The eluted 22 kDa protein product was dialyzed in storage buffer (10 mM HEPES, pH 7.4, 100 mM NaCl, 0.2 mM EDTA, 20% glycerol). Using this method the final protein yield was 0.7 g/l, and Bax was estimated to be at least 95% pure based on Coomassie Blue stained SDS-PAGE gels. EGFP-Bax purification was performed following the same protocol as that of wild-type Bax, with the additional precaution of wrapping the chitin column in an aluminum foil during the 48 h incubation period (final yield 0.4 g/l). To preserve activity, the protein was only frozen once at the end of the purification process. Single-cysteine Bax mutants were purified according to the same protocol and fluorescently labeled with diethylaminocoumarin (DAC), or nitrobenzofurazan (NBD) as previously described [50]. Recombinant full-length murine Bid with an N-terminal hexahistidine tag was expressed in *E. coli* and purified using a nickel-nitrilotriacetic acid-agarose column (Qiagen Inc., Mississauga, Ontario, Canada). Purified Bid was then cleaved using caspase 8 (Enzo Life Sciences, Exeter, UK). The C-terminal protein fragment (tBid) was separated from the N-terminal fragment, and from residual caspase 8, using affinity chromatography on a nickel-nitrilotriacetic acid-agarose column. The elution buffer contained the detergent octyl β-D-glucopyranoside (OG, 1.2% w/v). The eluted 15 kDa protein was concentrated in 10 mM $NaPO_4$ (pH 8.0), 300 mM NaCl, and 10% glycerol using an Amicon Ultra-15 centrifugal filter device (Millipore, Billerica, MA, USA). The final protein yield was 1.5 g/l, and tBid was estimated to be at least 95% pure based on Coomassie Blue stained SDS-PAGE gels.

2.3. Protein targeting assay

Samples containing different concentrations of liposomes and proteins (with a Bax-to-Bid ratio always equal to 5) were prepared in assay buffer with proteins added last. They were incubated for 2 h at 37 °C to ensure that equilibrium was reached, then brought back to room temperature. When working with fluorescent liposomes and EGFP-Bax, protein binding was assessed at that point using fluorescence correlation measurements. Subsequently membrane-bound proteins were separated from soluble proteins by gel filtration on a 2.5 ml Sepharose CL-2B column (Amersham Biosciences/GE Healthcare, Piscataway, NJ, USA). A total of 12 fractions (0.25 ml each) were collected. The protein concentration in each fraction was then assessed either by immunoblotting or again by fluorescence.

2.4. Immunoblotting

Fractions obtained after size-exclusion chromatography were run on SDS-PAGE gels. Proteins were detected by Western-Blot using the monoclonal Bax antibody 2D2 (a generous gift from Richard Youle) at a dilution of 1:10,000 [51], or the monoclonal tBid antibody 5C8 (Exalpha Biologicals, Shirley, MA, USA) at a dilution of 1:4000. A secondary antibody conjugated to horseradish peroxidase (Jackson ImmunoResearch Laboratories, West Grove, PA, USA) was used at a dilution of 1:10,000. Scanned immunoblots were analyzed using ImageJ [52]. The intensity of each fraction was evaluated from the image by converting the scanned blot to an 8-bit greyscale image, inverting the color, and subtracting the background intensity of the gel around each band. Membrane binding was quantified by comparing the summed intensities of membrane-bound fractions (fractions 1–5) with the total intensity from all protein fractions. A titration blot showed that in the range of Bax concentrations found in the different fractions collected after the column (~1 to ~50 nM), there was indeed a linear relationship between the amount of Bax present in a fraction and the signal detected (data not shown).

2.5. Fluorescence fluctuations experiments

2.5.1. Measurements

For fluorescence measurements samples were transferred to a 96-well microplate with a coverslip bottom (Whatman, Piscataway, NJ). Time-resolved fluorescence data was acquired and the corresponding autocorrelation function and photon counting histogram were computed using an Insight Research Spectrometer (Evotec Technologies, Hamburg, Germany) [53]. The fluorescence of EGFP-Bax and that of DiD-labeled liposomes was excited using continuous-wave laser diodes emitting at 488 nm and 635 nm, respectively, and collected in the "green" protein channel and the "red" liposome channel sequentially to avoid bleed-through between the two channels. The diameter of the excitation beams was set to be smaller than the objective back aperture, resulting in effective detection volume radii of 550 nm (green channel) and 680 nm (red channel), i.e. significantly larger than the liposomes that could then be considered as point particles during the analysis. The excitation power was 25 μW in each channel. This corresponds to a light flux of 2.6 kW/cm^2 at the sample for the green channel. In these conditions, the average time required to photobleach an EGFP fluorophore residing in the confocal detection volume is estimated to be 220 ms [54], i.e. significantly longer than the residence time of the liposome in the detection volume. For fluorescence intensity distribution analysis (FIDA) measurements, circular beam scanning with 45 μm radius and 20 Hz frequency was used to reduce photobleaching [53]. Measurements usually consisted of 4 individual 5 s runs. All measurements were performed at room temperature.

2.5.2. FCS analysis

The autocorrelation functions obtained for samples containing both EGFP-Bax and liposomes were analyzed (using the Acapella software, Evotec Technologies) assuming the presence of two independently diffusing fluorescent species, unbound EGFP-Bax and liposomes with bound EGFP-Bax. For this analysis, the diffusion time (i.e. average residence time in the confocal detection area) of unbound EGFP-Bax, $\tau_{D,1}$ ~0.5 ms, was fixed to that of the soluble monomeric protein obtained on the same day in a calibration step. The diffusion time of the liposomes, $\tau_{D,2}$, was left to vary and usually found to be between 5 and 20 ms. This analysis allowed for the retrieval of amplitudes A_1 and A_2, which correspond to the terms in the autocorrelation function associated to the diffusion of unbound EGFP-Bax and liposomes with bound EGFP-Bax, respectively. These amplitudes are related to the fraction, f, and the molecular brightness (i.e. average number of photons detected per second per particle), Q, of each species, according to $A_i = f_i Q_i^2 / (f_1 Q_1^2 + f_2 Q_2^2)$ [55]. An approximate value for the fraction of bound EGFP-Bax was then obtained using:

$$f_{bound}^{FCS} = A_2. \quad (1)$$

This simplified method of analysis results in an exact value for the fraction of bound EGFP-Bax when $Q_2 = Q_1$, (in which case $A_2 = f_2$), that is when there is one or less Bax molecule bound to each liposome, but it leads to an overestimate of the bound protein fraction when $Q_2 > Q_1$ (in which case $A_2 > f_2$).

2.5.3. FIDA

The photon counting histograms obtained from the fluorescence data were analyzed by FIDA using the Acapella software. FIDA returns the molecular brightness, Q, and the average number of flurophores in the detection volume, N, and can do so for different fluorescent species, as long as their molecular brightness is different [56]. As for FCS, the data collected in the "green" protein channel in the presence of both Bax-EGFP and liposomes was analyzed assuming the presence of two different species: unbound EGFP-Bax (with concentration N_1^{green} and with a molecular brightness, Q_1^{green}, fixed to that of soluble monomeric EGFP-Bax, i.e. Q_1^{green} ~8 kHz) and liposomes with bound EGFP-Bax (with concentration N_2^{green} and a molecular brightness, Q_2^{green}, left to vary, but always found to be larger than Q_1^{green}). The average number of EGFP-Bax molecules per liposome that carried at least one EGFP-Bax was then calculated as $n = Q_2^{green}/Q_1^{green}$, and the total EGFP-Bax concentration in the sample by $N^{green} = N_1^{green} + nN_2^{green}$. An estimate for the fraction of bound EGFP-Bax was obtained as:

$$f\frac{FIDA}{bound} = \frac{N_2^{green\,Q}{}_2 green \Big/ {}_Q 1^{green}}{N_1^{green} + N_2^{green\,Q}{}_2 green \Big/ {}_Q 1^{green}}. \quad (2)$$

This calculation returns an exact value of the fraction of bound EGFP-Bax when $Q_2 > Q_1$, i.e. when there is on average more than one EGFP-Bax bound to each liposome. When $Q_2 = Q_1$ (i.e. when there is one EGFP-Bax or less bound, on average, to each liposome), FIDA cannot distinguish between bound and unbound EGFP-Bax, and leads to an underestimate of the fraction of bound EGFP-Bax.

The photon counting histograms associated with the data collected in the "red" liposome channel were also analyzed by FIDA and used to find the exact concentration of liposomes in each sample, N^{red} – during this analysis, the molecular brightness of a single liposome was fixed to the value Q^{red} determined in a calibration sample containing only liposomes. From there, the fraction of liposomes carrying EGFP-Bax molecules could be calculated ($F = N_2^{green}/N^{red}$) along with the exact Bax-to-liposome ratio ($r_{measured} = N^{green}/N^{red}$). The value of r obtained in this way always represents a very accurate and robust measurement of the Bax-to-liposome ratio – because it is essentially based on the average values of the fluorescence signal in the green and red channels.

Actual protein and liposome concentrations, c, were obtained from N^{green} and N^{red}, respectively, using $c = NV_0$, where the value of the confocal volume is $V_0 = 10$ fl (obtained by performing calibration experiments with fluorescent dyes).

2.5.4. Simple model for Bax binding to liposomal membranes

The observed binding of Bax to liposomal membranes was compared to the predictions of a basic binding model, where one assumes a partition of Bax between the solution and the membranes according to the simple equilibrium: $P_{bound} = KLP_{free}$ [57]. K is the molar partition coefficient or apparent association constant between protein and lipid, L is the lipid concentration, and P_{bound} and P_{free} are the concentrations of bound and unbound Bax proteins, respectively. The fraction of bound Bax then depends on the Bax-to-lipid ratio, P/L, according to:

$$f_{bound} = \frac{KP}{KP + (P/L)} = \frac{KL}{1 + KL}, \quad (3)$$

where P is the total Bax concentration.

The ratio of bound Bax protein to liposome can then be calculated as $m(P/L)f_{bound}$, where m is the number of lipids per liposome. At high P/L at least, a random distribution of Bax on the liposomes can be expected. In this case the fraction of liposomes carrying at least one Bax, $f^L{}_{bound}$, and the average number of Bax bound per liposome carrying at least one Bax, n, both quantities that can be measured by FIDA as explained above, can be calculated as:

$$f^L_{bound} = 1 - e^{-\frac{mKP}{1+KL}} \quad (4)$$

and

$$n = \frac{mKP/(1+KL)}{1 - e^{-mKP/(1+KL)}}. \quad (5)$$

As long as $L \ll 1/K$, n tends towards the limit value $mKP/(1-e^{-mKP})$ at high P/L. On the other hand, if $L \gg 1/K$, then n tends towards $mP/L = r$ at high P/L.

2.6. Bax oligomerization assay

Bax oligomerization in the membrane of liposomes was assessed by detecting the fluorescence resonance energy transfer (FRET) between a single cysteine mutant of Bax (Bax134C) labeled with DAC and a single cysteine mutant of Bax (Bax126C) labeled with NBD, as described previously [50]. Briefly, liposomes were incubated with DAC-134-Bax (donor), NBD-126-Bax (acceptor) in excess and tBid (with a 1 to 5 tBid to Bax ratio). The background fluorescence, F_B, was first measured in the absence of the proteins, then proteins were added and the fluorescence of the donor, $F(t)$, was monitored as a function of time ($\lambda_{ex} = 383$ nm, $\lambda_{em} = 463$ nm) using a microplate reader (M1000, Tecan, Durham, NC, USA). The reduction in fluorescence due to FRET was assessed by considering the normalized donor fluorescence: $(F(t) - F_B)/(F(0) - F_B)$. In each case control experiments were performed using solutions without liposomes and solutions where NBD-126-Bax was replaced with unlabeled Bax (i.e. without acceptor).

2.7. Membrane permeabilization assay

2.7.1. ANTS release assay

The capacity of the purified proteins to permeabilize membranes was tested using an ANTS release assay, where the dequenching of the fluorophore 8-aminonaphthalene 1,3,6-trisulfonic acid (ANTS) is monitored as it is released from the liposomes, which also contain the quencher p-xylene-bis-pyridinium (DPX) [17]. The ANTS/DPX liposomes were prepared by supplementing the buffer used to resuspend lipid films with 12.5 mM ANTS and 45 mM DPX (both purchased from Molecular Probes, Eugene, OR, USA), and then removing the non-encapsulated ANTS and DPX by gel filtration over a CL2B-Sepharose column (Amersham Biosciences, Piscataway, NJ, USA). When required in order to precisely quantify liposome concentration, DiD was added to the lipids as explained above. The ANTS fluorescence emission ($\lambda_{ex} = 355$ nm, $\lambda_{em} = 530$ nm) from solutions containing different amounts of liposomes and recombinant proteins was monitored using an Envision spectrofluorometer (Perkin Elmer, Waltham, MA, USA). Samples with varying lipid concentrations were prepared using a fixed amount (50 μM lipid) of ANTS/DPX liposomes and varying amounts of liposomes without ANTS or DPX, in assay buffer. For each sample the average background fluorescence (F_0) was first measured for 30 min in the absence of proteins. Recombinant proteins (i.e. Bax and tBid) were then added at the appropriate concentration, and the ANTS fluorescence, $F(t)$, was monitored. After 2 h, Triton X-100 was added to a final concentration of 0.2% – to promote liposome lysis – and the average maximum fluorescence (F_{100}) was measured over a period of 10 min. The percentage release of ANTS/DPX was calculated as $R(t) = [(F(t) - F_0)/(F_{100} - F_0) - (F'(t) - F'_0)/(F'_{100} - F'_0)] \times 100$, where

F' was the signal in the absence of added protein. All measurements were performed at room temperature.

2.7.2. Determination of the Bax binding equilibrium constant from ANTS release data

To determine the equilibrium constant for Bax binding to liposomes, K, we followed the approach described by Grant et al. [58]. For a simple partition equilibrium, $P_{bound} = KLP_{free}$, the conservation equation for Bax can be written $P = P_{bound}(1 + 1/KL)$. A particular amount of permeabilization (defined here as a particular amount of ANTS release in the long time limit, R_i) can be expected to be achieved for a particular number of bound Bax proteins per liposome, n_i, that is for a particular value of $P_{bound}/L = n_i/m$. Therefore the Bax concentration necessary to obtain a given R_i is $P(L) = n_i m(1/K + L)$.

The values of R (i.e. the percentage of ANTS release after 2 h) obtained experimentally at a given lipid concentration for different Bax concentrations were fitted with a simple exponential function:

$$R(P) = R_{\max}\left(1 - e^{-P/P^*(L)}\right), \tag{6}$$

where R_{max} is the maximum release obtained in the assay. A specific R_i can be obtained by using any combination of P and L that obeys: $P = \ln[R_{max}/(R_{max} - R_i)]P^*(L)$. By identification with the Bax conservation equation obtained above, in the case of a simple partition equilibrium we thus expect $P^*(L)$ to depend linearly on L: $P^*(L) = a + bL$, with $K = b/a$ and $s_i = b\ln[R_{max}/(R_{max} - R_i)]$.

2.8. Small angle neutron scattering

2.8.1. Experiments

SANS measurements were primarily carried out at the National Institute of Standards and Technology (NIST, Gaithersburg, MD) 30 m NG3 SANS instrument [59]. A 12 m sample-to-detector distance (SDD) was used along with a neutron wavelength $\lambda = 8$ Å, and $\lambda = 5.5$ Å for SDDs of 4 and 1.3 m, resulting in a total range in scattering vector ($q = 4\pi \cdot \sin(\theta/2)/\lambda$, where θ is the scattering angle) of $0.003 < q < 0.5$ Å^{-1}. Neutron wavelengths were selected using a mechanical velocity selector with an 11% full-width-at-half-maximum (FWHM) energy dispersion. Samples containing lipids and proteins were prepared in assay buffer with the appropriate amount of D_2O, and incubated at room temperature for 1 h. Samples were then placed in standard 2 mm-path-length quartz cells. Data were collected using a 640 mm × 640 mm 2D ^{3}He position-sensitive detector with a 5 mm × 5 mm resolution. Acquired images were corrected using a suite of software supplied by NIST [60]. Additional measurements were carried out at Oak Ridge National Laboratory (ORNL, Oak Ridge, TN) using the Bio-SANS instrument that is located at the ORNL High-Flux Isotope Reactor (HFIR). A neutron wavelength $\lambda = 6$ Å with a 14.5% FWHM energy dispersion was used together with SDDs of 2.5 m and 15.3 m.

In the case of lipid dispersions, the scattering from water makes a substantial contribution to the total scattered intensity and must be subtracted. Every data set was normalized using the measured transmission, T, defined as the ratio of the direct beam passing through the sample cell containing either lipids and proteins dispersed in buffer, $I_{S+W}(0)$, or only buffer, $I_W(0)$, to the direct beam passing through an empty sample cell, $I_B(0)$, i.e., $T_{S+W} = I_{S+W}(0)/I_B(0)$. The scattering from the sample itself was then calculated on an arbitrary scale as $I_S(q) = I_{S+W}(q)/T_{S+W} - I_W(q)/T_W$.

2.8.2. Analysis of scattering data

SANS data were analyzed using either a one-strip or a two-strip asymmetric model based on the multi-strip models developed by Kučerka et al. [61]. Liposome polydispersity was taken into account by convoluting the model with the Schulz distribution function [62]. We assume a nonspecific association of liposomes, which predicts an almost unitary interparticle structure factor. This has been confirmed experimentally for neutral unilamellar liposomes at total lipid concentrations <3 wt.% [63]. In the case of the one-strip model, each liposome is represented by a spherical shell of thickness t and radius R (measured from the center of the strip), with constant scattering length density (SLD). In the case of pure liposomes, the shell represents the hydrophobic part of the bilayer, while in the case of liposomes with proteins either at the protein contrast match point or at the lipid contrast match point, the shell represents the hydrophobic part of the lipid bilayer, or the protein layer, respectively. In the case of the asymmetric two-strip model, each liposome is represented by two concentric spherical strips with constant SLDs. The inner strip represents the lipid bilayer, eventually containing proteins, while the outer strip represents the protein protruding beyond the lipid bilayer. The variable parameters in this model are: liposome radius (R is measured from the center of the lipid bilayer); lipid thickness (t_L) and lipid bilayer SLD (s_L); protein thickness (t_P) and SLD (s_P) of the protruding protein layer; and liposome polydispersity (s). The error on the retrieved parameters was calculated from the covariance matrix coefficients multiplied by the square root of the total chi-square. All fits to the data include the instrumental resolution ($\Delta\lambda/\lambda = 11\%$), with sample polydispersity having the most pronounced effect in "smearing" the SANS data. Nevertheless, under the present experimental conditions and for the systems in question, the technique is sensitive to relative changes of a few angstroms.

3. Results

3.1. Bax targeting to liposomes saturates at high protein-to-lipid ratios

To evaluate what percentage of Bax molecules binds to liposomes and establish the functionality of the small (50 nm diameter) biomimetic mitochondrial liposomes used in the SANS experiments reported below, a series of membrane targeting experiments was performed. First, different amounts of Bax activated by tBid (with a Bax-to-tBid ratio kept constant and equal to 5) were incubated with different liposome concentrations, after which liposome bound proteins were separated from free proteins by gel filtration and detected using immunoblotting. Liposomes consistently eluted in earlier fractions (fractions 2 to 5), as shown by using fluorescent and by measuring the fluorescence signal in each fraction (Fig. 2A). In contrast, free Bax proteins (in the absence of liposomes) consistently eluted in later fractions (6 and above, immunoblotting data not shown). The Western-Blots obtained for one particular series of targeting experiment are shown in Fig. 2B, where 100 nM wtBax and 20 nM tBid were incubated with varying amounts of liposomes in order to obtain a Bax-to-liposome ratio before gel filtration comprised between r = 1 and r = 50 (an estimated value of r based on the total lipid and protein amounts used to prepare the samples). Strikingly, while at low Bax-to-liposome ratios the majority of Bax protein was found in fractions 2 to 5 (i.e. bound to liposomes), as r was increased, an increasing fraction of Bax appeared in fractions 6 and above (i.e. not bound to liposomes). This was observed both at low (Fig. 2, Bax concentration 100 nM) and at high protein concentrations (Table 1, Bax concentration 10–30 μM, i.e. similar to that used in the neutron scattering experiments described below). In contrast, immunoblotting against tBid showed that for all proteins-to-liposome ratios explored, about 90% of tBid was associated with the membrane (data not shown). The fact that Bax binding to liposomal membranes saturated at high r was a robust feature observed in all of the membrane targeting experiments performed. However, the fraction of bound Bax estimated from the immunoblots for a given r varied considerably from experiment-to-experiment (e.g. between 50 and 80% at r ~1, and between 0 and 20% at r ~50), despite efforts to work within the linear response range of the technique.

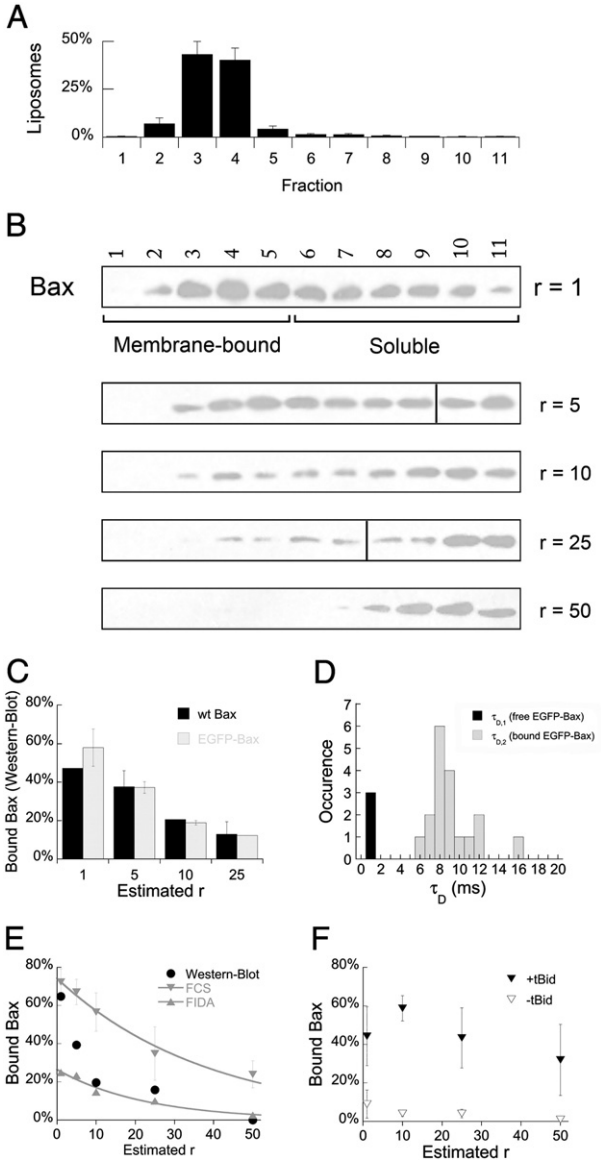

Fig. 2. Bax targeting to liposomal membranes. Western-Blot and fluorescence analysis of the different fractions obtained after gel-filtration of samples containing wtBax or EGFP-Bax incubated with liposomes in the presence or in the absence of the activating protein tBid. (A) Elution profile of the liposomes (fluorescently labeled with DiD) as obtained from the recorded fluorescence signal in each fraction (average ± stdev, n = 5). (B) Representative elution profile of Bax in the presence of tBid at different Bax-to-liposome ratios obtained by Western-Blot (wtBax concentration: 100 nM, tBid concentration: 20 nM). (C) Comparison between the binding of wtBax and EGFP-Bax, as observed by Western-Blot. (D) Distribution of residence times observed for liposomes carrying EGFP-Bax shown for one representative FCS experiment. (E) Percentage of Bax bound to liposomes versus r, as measured by Western-Blot, FCS and FIDA (EGFP-Bax: 100 nM, tBid: 20 nM). Only one representative series of measurements is shown (for fluorescence measurements: average ± stdev, n = 10). (F) Comparison of Bax binding in the presence and absence of tBid, as measured by FCS (EGFP-Bax: 100 nM, tBid, when present: 20 nM). Only one representative series of measurements is shown (average ± stdev, n = 10).

Immunoblotting requires bound and unbound proteins to be separated by gel filtration. The technique therefore cannot clearly distinguish between proteins inserted into the membrane and proteins peripherally bound to the membrane – the latter may or may not unbind from the liposomes during gel filtration. In contrast, fluorescence fluctuation methods, which are performed directly in solution, detect all membrane-bound proteins whether inserted or peripherally bound (just as the SANS experiments described below). We therefore used both fluorescence correlation spectroscopy (FCS) and fluorescence intensity distribution analysis (FIDA) to further characterize Bax targeting to liposomal membranes. For this, EGFP-Bax was used instead of wtBax, allowing us to detect the protein via its fluorescence emission – immunoblotting experiments showed that the membrane targeting of EGFP-Bax is indistinguishable from that of wtBax (Fig. 2C), while ANTS release experiments showed that the pore-forming activity of EGFP-Bax is only slightly lower than that of wtBax (see Section 3.5 below). With FCS the distinction between bound and unbound proteins is made based on diffusion properties (i.e. proteins bound to liposomes have a diffusion constant more than 10-fold lower – and therefore a residence time in the confocal detection volume more than 10-fold higher – than free proteins, see Fig. 2D). With FIDA the same distinction is made based on specific brightness, i.e. on the number of photons per second emitted by a diffusing particle (unbound EGFP-Bax proteins have a specific brightness exactly equal to that of a single EGFP fluorophore, while liposomes with bound EGFP-Bax proteins have a specific brightness equal to or greater than that of a single EGFP fluorophore, depending on the number of EGFP-Bax bound to the liposome). For both fluorescence methods, the fraction of bound Bax was calculated in a simple but approximate way, where the value f_{bound}^{FCS} calculated from FCS analysis (Eq. (1)) is correct only at low r, and is an overestimate at high r, while the value f_{bound}^{FIDA} calculated from FIDA (Eq. (2)) is correct only at high r and is an underestimate at low r (see Materials and methods for more details). For a typical series of targeting experiments the fraction of bound Bax, as estimated with each of these three methods (immunoblotting, FCS and FIDA), is shown in Fig. 2E. As expected, while both FCS and FIDA show the same decreasing trend as observed with immunoblotting, the FCS estimates are close to the immunoblotting results only at low r (and always higher), while the FIDA estimates are close to the immunoblotting results only at high r (and always lower). In the case of a random distribution of the proteins on the liposomes, one should be able to calculate the exact percentage of bound protein from either the FCS or the FIDA data [64]. However, it has been shown that Bax oligomerization is a cooperative process [12], therefore the assumption of a random distribution of Bax on the liposome is likely wrong at low protein-to-liposome ratios. Also, while in theory FCS and FIDA results could be combined to obtain the correct bound fraction of Bax, in practice this becomes intractable if there is a large number of fluorescent species in solution with different brightness, most likely the case here. Importantly, however, even this simple approximate analysis (Eqs. (1) and (2)) is sufficient to demonstrate a few important points beyond the saturation effect observed, as will be shown in the next three sections.

3.2. Bax does not bind to liposomal membranes in the absence of tBid

Immunoblotting suggests that in the absence of tBid, less than ~10% of Bax or EGFP-Bax is stably bound to liposomes (data not shown and [50]). However, this does not rule out the possibility that some Bax may transiently bind to membranes in the absence of tBid, an interaction that could be disrupted during gel filtration. Indeed, the presence of lipid membranes alone can induce a transient Bax conformational change [17], and in healthy cells a small fraction of Bax is found loosely associated with mitochondrial membranes (as shown by the fact that this fraction is carbonate extractable) [10,32]. Because it is so extremely sensitive to the presence of bound proteins and because it can be used in the absence of any gel filtration, FCS offers the possibility to test for the presence of loosely bound proteins interacting transiently with liposomes – as long as the interaction lasts for more than a few ms, thus visibly slowing down the diffusion of the interacting proteins. However, when observing the diffusion of the EGFP-Bax in the presence of liposomes, but in the absence of tBid (Fig. 2F), it appeared that the total amount of EGFP-Bax associated with the liposomes is always less than 5% (for r > 1), or that the interaction is too transient (lasting less than a few ms) to be detected by FCS.

Table 1
Liposome structural parameters, Bax membrane targeting, and Bax membrane permeabilization capacity measured for the different Bax-to-liposome molar ratios explored by SANS.

Neutron Contrast	Estimated Bax concentration[a]	Estimated tBid concentration[a]	Estimated lipid concentration[a]	Glycerol content[a]	Estimated Bax-to-lipid ratio, P/L[b]	Estimated Bax-to-liposome ratio, r[b]	Membrane bound Bax (%)[c]	Estimated bound Bax-to-lipid ratio[d]	Estimated bound Bax-to-liposome ratio[e]	Membrane permeabilization[f]	Average liposome radius, <R> (nm)[g]	Polydispersity, s/<R>[h]	Lipid bilayer thickness, t_L (nm)[g]	Protein layer thickness, t_P (nm)[g]
0–40% D_2O	0	0	5.3–12.7 g/l 6.9–16.5 mM	0%	0	0		0	0	No	23.7 ± 0.2	0.24	3.8 ± 0.1	
15, 40 and 60% D_2O	0.27 g/l 12 μM	0.037 g/l 2.5 μM	17 g/l 22 mM	7.9%	1:1800	12	54% 38 ± 8% ~60%	1:3300 1:4700 1:3000	6 5 7 ~10–15	Yes	27.7 ± 0.2	0.24	3.4 ± 0.1	5.0 (fixed)
15, 40 and 60% D_2O	0.27 g/l 12 μM	0.037 g/l 2.5 μM	7.3 g/l 9.5 mM	8.1%	1:800	27	57% 20 ± 2% ~40%	1:1400 1:4000 1:2000	15 5 11 ~10–15	Yes	27.0 ± 0.2	0.35	3.4 ± 0.1	5.0 (fixed)
15, 40 and 60% D_2O	0.54 g/l 25 μM	0.073 g/l 4.9 μM	7.3 g/l 9.5 mM	15.8%	1:400	54	20% 12 ± 6% ~20%	1:1900 1:3300 1:2000	11 6 11 ~10–15	Yes	27.5 ± 0.2	0.28	3.3 ± 0.1	5.0 ± 1.2

[a] The protein, lipid and glycerol concentrations listed for the last three samples correspond to those in 15% D_2O buffer. 40% and 60% D_2O samples were prepared by diluting 15% D_2O samples, resulting in lower protein and lipid concentrations, but the same Bax-to-liposome ratios.

[b] Bax-to-lipid and Bax-to-liposome ratios were estimated from the amounts of protein and lipid used to prepare the samples, that are listed in columns 1 and 3.

[c] The percentage of membrane bound Bax was estimated in three ways for each different r: (i) using a gel filtration targeting assay at the same protein, lipid and glycerol concentration as listed in the table for 0% D_2O (first line); (ii) using a gel filtration targeting assay at lower protein concentration (100 nM Bax), but the same r as listed in the table (second line); (iii) using the FIDA data shown in Fig. 3A, assuming that the estimated and measured r values were the same (third line).

[d] Bound Bax-to-lipid ratios were estimated from the percentages of membrane bound Bax listed in the previous column.

[e] Bound Bax-to-liposome ratios were estimated from the listed percentages of membrane bound Bax (first three lines) or directly from the FIDA data shown in Fig. 3C, assuming that estimated and measured r were the same (fourth line).

[f] Membrane permeabilization was assessed using ANTS release for samples prepared with the indicated amount of protein, lipid and glycerol (0% D_2O).

[g] Structural parameters were obtained by global fit analysis of different SANS scattering curves recorded at a given Bax-to-liposome ratio, using either the one-strip (r = 0) or two-strip model (r = 12, 27 and 54).

[h] s/<R> is the size polydispersity of the liposomes.

3.3. In the presence of excess tBid, Bax binding to liposomes can for the most part be described in terms of a simple partition between the solution and the membranes

Fluorescence measurements performed on samples where both a fluorescent protein (EGFP-Bax) and fluorescently labeled liposomes (containing a small amount of the lipophilic dye DiD) were used, allowed for the determination of precise Bax, liposome and lipid concentrations. This in turn allowed for the calculation of the exact Bax-to-liposome ratio (noted "measured r" in the following, as opposed to the "estimated r" calculated from the protein and lipid masses used to produce the sample that was discussed above). It was found that the measured r was often higher than the estimated r, with large variations observed from preparation-to-preparation. This discrepancy was mainly the result of a lipid concentration that was lower than expected, showing that during the resuspension and extrusion steps, not unexpectedly a significant amount of lipid was not incorporated into liposomes. This is one reason why different repeats of the same experiment might give different values for bound Bax, since this value depends on r, and the actual r can vary from experiment-to-experiment.

To test for the real dependence of the fraction of bound Bax on r, we performed a series of experiments where solutions were prepared with EGFP-Bax and fluorescently labeled liposomes (both with 50 nm and 100 nm diameters – larger liposomes might not behave as point objects in FIDA experiments and were not used), with an estimated r ranging from 1 to 50 (as previously) and with a Bax-to-tBid ratio of 5 (i.e. with tBid-to-liposome ratios ranging from 0.2 to 10). After incubation these solutions were separated into different fractions by gel filtration. The actual Bax concentration (P) and lipid concentration (L) were measured by fluorescence for each sample before gel-filtration, and for each fraction of each sample after gel filtration, allowing to calculate the exact Bax-to-liposome ratio for each sample, which was found to vary from r ~1 to r ~100. In parallel, FIDA was used to measure the fraction of bound Bax in each of these samples before and after gel filtration (shown as a function of L, r and P/L in Fig. 3A–D), as well as the percentage of liposomes carrying any Bax (Fig. 3E–F), and the average number of Bax per liposome (Fig. 3G–H).

Focusing first on the experiments done with 50 nm diameter liposomes (Fig. 3A, C, E, G), the following was observed. For all samples with a Bax-to-liposome ratio 5 or larger before gel filtration (i.e. with an initial tBid-to-liposome ratio larger than 1), the different fractions collected after the gel filtration column had a percentage of bound Bax that seemed uniquely dependent on lipid concentration (Fig. 3A), and generally in good agreement with a simple partition equilibrium model (Eq. (3)), especially considering that the measured value of the bound fraction measured by FIDA is only exact at high r (i.e. at low L). When less than one tBid molecule per liposome was present (initial $r<5$), the amount of bound EGFP-Bax still roughly followed a simple partition equilibrium but with a lower apparent association constant ($K=0.08\pm0.02\ \mu M^{-1}$ for initial $r=1$, to be compared with $K=3.5\pm0.4\ \mu M^{-1}$ in the presence of excess tBid, as measured for the experiment shown in Fig. 3A). When considering the dependence of Bax binding on Bax-to-liposome ratio instead of L, we found that within the spread of the data r was also a good predictor of the amount of bound Bax (Fig. 3C), of the percentage of liposomes with Bax (Fig. 3E) and of the number of Bax per liposome (Fig. 3G), where the amount of bound Bax monotonously decreases as r increases while the amount of liposomes carrying any Bax progressively increases, in agreement with what was observed by immunoblotting. Interestingly, the data obtained before gel filtration is slightly different, with lower amounts of binding and fewer liposomes carrying any Bax, but with more Bax molecules per liposome (Fig. 3A, C, E, G). We attribute this to the possibility that there might be an inactive EGFP-Bax fraction that remains on the column (the amount of protein recovered from the column is never 100%) and that samples were only incubated for 2 h before gel filtration, while samples after gel filtration were incubated for longer periods of time because of the difficulty in measuring different fractions quickly.

3.4. Bax binds to liposomes of different sizes

To directly compare the binding of Bax to liposomes of different sizes, the data obtained for 50 nm and 100 nm liposomes were plotted together as a function of protein to lipid ratio (Fig. 3B, D, F, H). Both at the same L and at the same P/L, a slightly higher fraction of Bax binds to 50 nm liposomes than to 100 nm liposomes. This effect was quantified by assuming a simple partition equilibrium between soluble and membrane bound Bax. First the obtained values of f_{bound} (for $r>10$ since that is the range in which FIDA data are exact) were fitted as a function of L with Eq. (3), returning an apparent association constant $K=3.0\pm0.4\ \mu M^{-1}$ for 50 nm diameter liposomes and $K=1.3\pm0.2\ \mu M^{-1}$ for 100 nm diameter liposomes (Fig. 3B, considering the data of two separate experiments). Second, to explain the dependence of the data on r and P/L, and in particular the observed saturation of the number of bound Bax per liposome at high r, the obtained values of f_{bound} (for $P/L>10/m$, i.e. $P/L>0.0005$ and 0.00012 for 50 nm and 100 nm diameter liposomes, respectively) were fitted with Eq. (3) as a function of P/L. Since f_{bound} is expected to depend on P as well as on P/L, portions of the data for which $0.002\ nM<P<0.01\ nM$ and $0.2\ nM<P<1\ nM$ were selected, and separate fits were performed for these two subsets of data, returning separate values for KP. Subsequently K was calculated using the average value of P for each subset of data. This way, $K=2.4*10^6\ M^{-1}$ to $6.3*10^6\ M^{-1}$ was obtained for Bax binding to 50 nm liposomes, and $K=0.8*10^6\ M^{-1}$ to $2.9*10^6\ M^{-1}$ for Bax binding to 100 nm liposomes. The fact that K seems to depend on P indicates that the partition model used to analyze the data only approximately describes the behavior of the system. Strikingly, however, the values of K obtained in a given P range were always higher for the smaller liposomes. Using these values to predict the percentage of liposomes carrying bound Bax (Fig. 3F) and the average number of bound Bax per liposome carrying Bax (Fig. 3H), we found that the agreement with the FIDA data was poor at low P/L, but reasonable as expected at high P/L. In particular, the measured association constants could be used to predict that, at the Bax concentrations found in these samples (mainly $0.01\ nM<P<1\ nM$), the number of bound Bax per liposome should saturate above P/L ~0.001 reaching ~10 for 50 nm liposomes and ~20 for 100 nm liposomes, in fair agreement with the experimental data.

3.5. Bax activated by tBid oligomerizes and permeabilizes the membrane of liposomes of different sizes in a concentration-dependent manner

To check the membrane permeabilization activity of Bax under the conditions of the SANS experiments discussed below (i.e. with 50 nm diameter liposomes at high protein concentrations and high protein-to-liposome ratios), several control experiments were performed. First, a Bax-Bax FRET assay was carried out to verify that Bax did oligomerize in the membrane of liposomes with small (50 nm) diameter. Donor Bax (20 nM, labeled with DAC) was incubated with excess acceptor Bax (100 nM, labeled with NBD) in the presence of tBid (24 nM) and either 50 nm, 100 nm or 200 nm diameter liposomes. The liposomal membranes were labeled with DiD, so that it could be ensured that the exact same lipid concentration (estimated at 0.055 g/l or 70 μM) was present in all incubations. The donor Bax fluorescence was found to decrease over time to a roughly similar extent in all cases (Fig. 4). On the other hand, when the acceptor Bax was replaced with unlabeled Bax, the donor Bax fluorescence remained constant (Fig. 4, shown only for 100 nm diameter liposomes). Thus the observed decreased donor fluorescence in the presence of acceptor is due to FRET and faithfully reflects Bax oligomerization. This data show that Bax oligomerization is as efficient in small 50 nm diameter liposomes as it is in larger 200 nm liposomes.

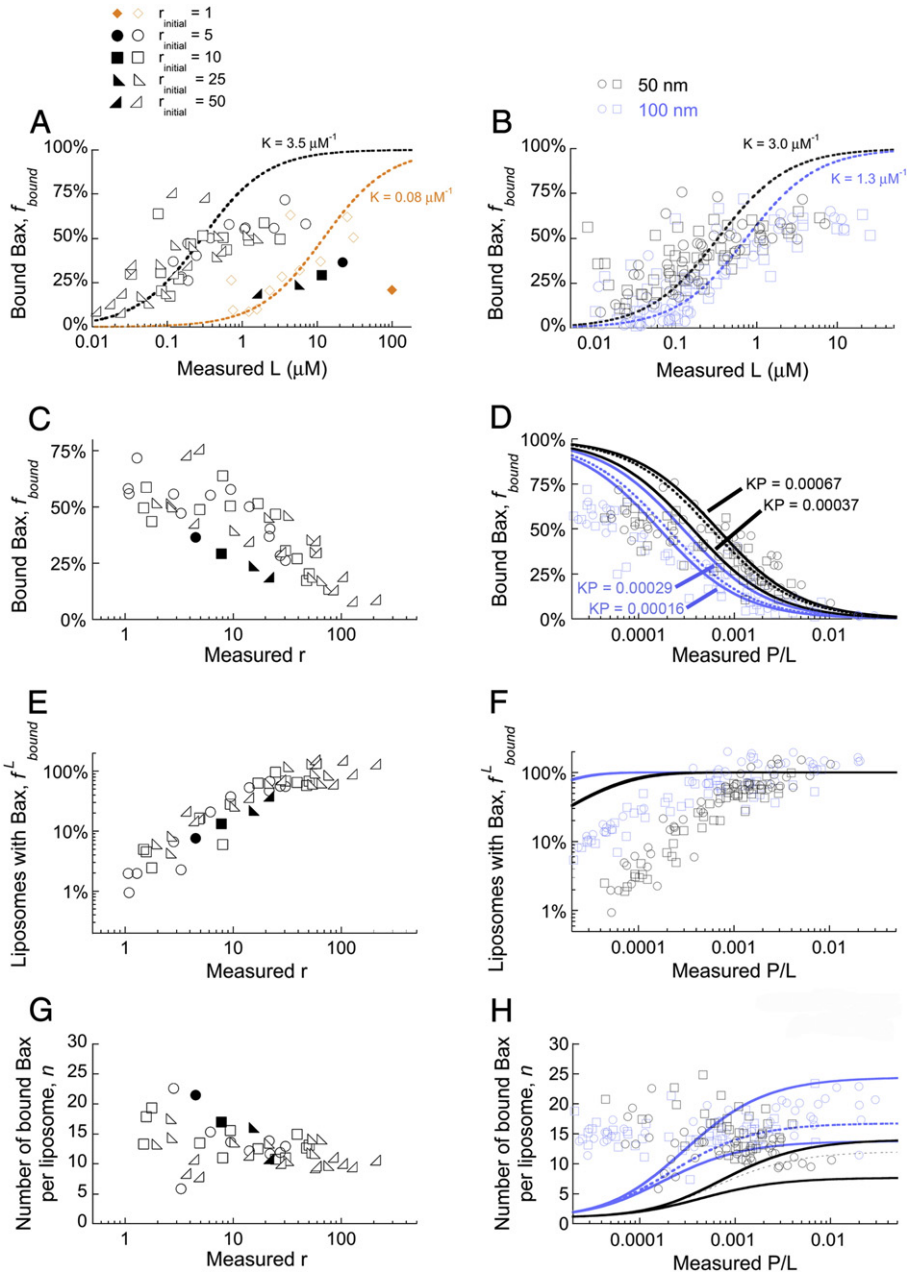

Fig. 3. Quantification of Bax targeting to liposomal membranes using FIDA. (A–D) Percentage of bound Bax, (E, F) percentage of liposomes with bound Bax, and (G, H) average number of Bax molecules per liposome as a function of: (A, B) the measured lipid concentration, (C, E, G) the measured Bax-to-liposome ratio or (D, F, H) the measured Bax-to-lipid ratio. The values of *L*, *r* and *P*/*L* were calculated directly from the fluorescence data. In (A, C, E, G), solid symbols correspond to data obtained before gel-filtration, and open symbols to data obtained after gel filtration for different fractions. The value $r_{initial}$ appearing on the figure legend is the value of r before gel filtration, as estimated from the quantities of protein and lipid used to prepare the samples. Since all samples were prepared with a Bax-to-tBid ratio of 5 and since the entire tBid population binds to liposomes, the number of tBid per liposome can be estimated to be $r_{initial}/5$. In (B, D, F, H), data is shown for 50 nm diameter liposomes (black symbols) and 100 nm diameter liposomes (blue symbols), and circle and square symbols represent different repeats of the experiments (without distinguishing between different $r_{initial}$). In (A, B, D), lines represent fit of the data with Eq. (3), where the dashed lines are fit of all data point for which $r > 10$, while the solid lines are fit of only subsets of these same data points grouped according to Bax concentration (0.1 nM$<P<$0.5 nM and 1 nM$<P<$5 nM). In (F) and (H), lines represent expected values according to Eqs. (4) and (5), respectively, using the values of *KP* obtained from the fit in (C).

Second, ANTS release experiments were performed both at low lipid concentrations (0.04 g/l, allowing for low background scattering) for a larger range of protein-to-liposome ratios (estimated r = 8 to 82) and at high lipid concentrations under the same conditions as the SANS experiments. The experiments carried out at low lipid concentration (Fig. 5A) show that the amount of ANTS released from the liposome increases with Bax concentration at low protein concentration, but reaches a maximum value of ~80% ANTS release for ~100 nM Bax, i.e. r ~40 (the assay likely ends at 80% rather than 100% due to increased ANTS fluorescence in the micelles formed by the lipids and by the detergent used to lyse the liposomes). Although a large amount of scattering was present in the highly concentrated protein and lipid samples, making it difficult to obtain a quantitative estimate of the percentage of ANTS release, it appeared that when activated by tBid, Bax exhibited membrane permeabilization characteristics for all conditions explored (Table 1), resulting in about 80% of the ANTS to be released for r = 54 (Fig. 5B). This result is consistent with those obtained at low lipid concentrations. However, at high lipid and protein concentrations, Bax resulted in some ANTS release even in the absence of tBid. Taken together, these release experiments show that for 50 nm diameter

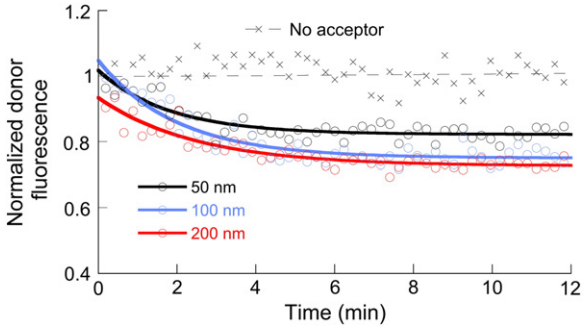

Fig. 4. Bax oligomerization. Normalized DAC-134-Bax (donor) fluorescence recorded when incubating liposomes of different diameters with 20 nM DAC-134-Bax, 100 nM NBD-126-Bax and 24 nM tBid. In all cases, the estimated P/L was 0.0017. The normalized fluorescence obtained when the acceptor (NBD-126-Bax) was replaced by unlabeled Bax (i.e. in the absence of acceptor) is also shown for 100 nm diameter liposomes (crosses). Lines are exponential fit of the data.

liposomes and for estimated Bax-to-liposome ratios larger than 15, after a 2 hour incubation most liposomes carry at least one Bax pore, resulting in 50% or more ANTS release (Fig. 5C).

Third, the amount of ANTS release obtained for different size liposomes was compared. We used DiD-labeled liposomes in order to ensure that, even if reliable absolute values of the lipid concentration could not be achieved, relative values of r were reliably obtained (for this the fluorescence of DiD was measured in each sample and liposome concentrations were adjusted in order to obtain samples with liposomes of different sizes and the exact same lipid concentration). We observed that the amount of ANTS release was significantly higher for smaller liposomes at a given r (Fig. 5C), but comparable for liposomes of all sizes at a given P/L (Fig. 5D). Using 100 nm diameter liposomes, we also checked that the EGFP-Bax fusion protein used for the fluorescence fluctuation data presented above was able to permeabilize membrane (Fig. 5C). Although the amount of ANTS release obtained for EGFP-Bax at a given r is not as high as for wtBax, the fluorescence fusion protein is still able to efficiently permeabilize membranes.

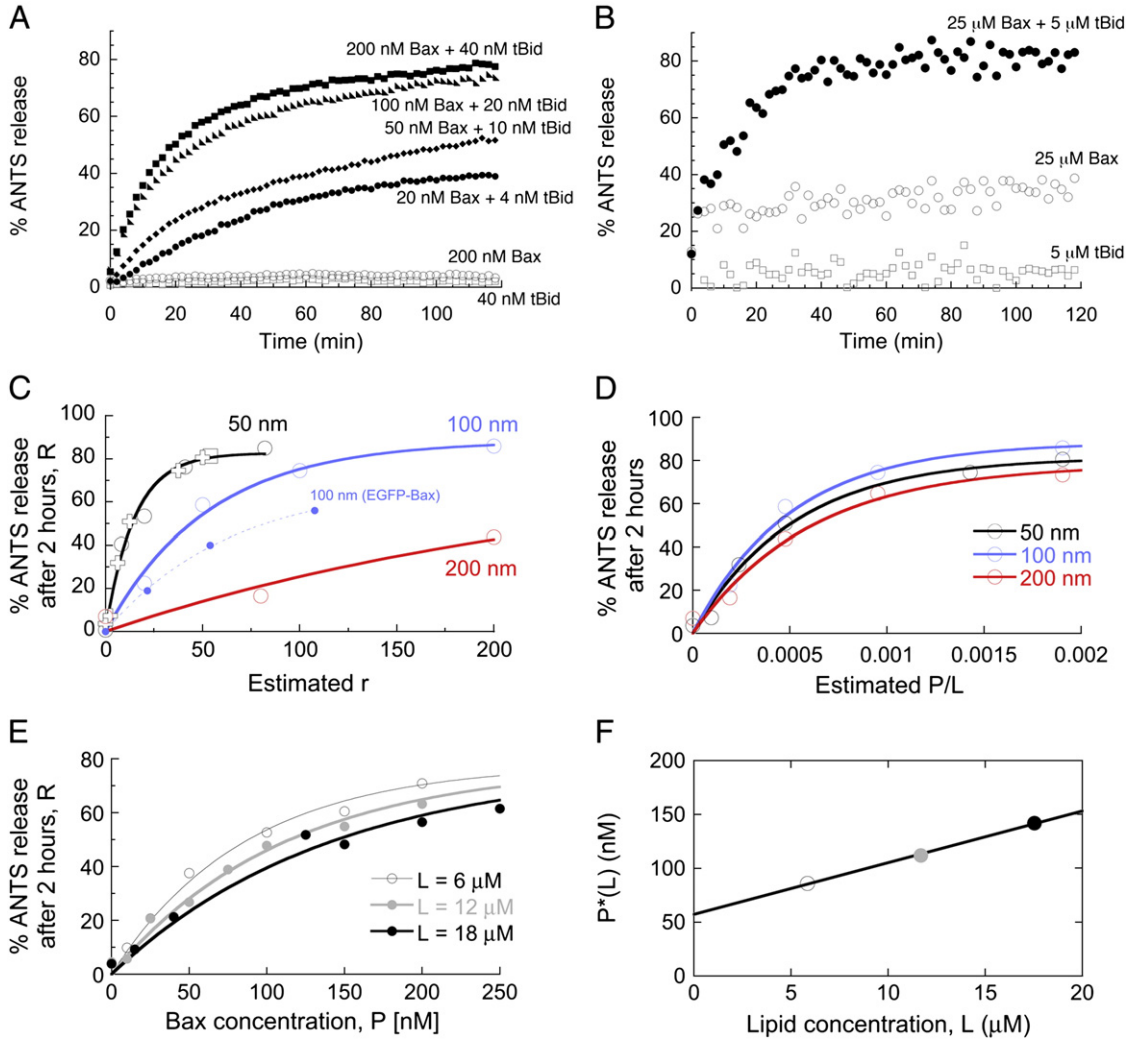

Fig. 5. Bax membrane permeabilization activity. Comparison between the percentage of ANTS release obtained (A) at low lipid and protein concentrations (for different r between 8 and 82) and (B) at high lipid and protein concentrations (r = 54). In each case, the percentage of release is shown when liposomes were incubated with both Bax and tBid in a ratio of 5 to 1 (solid symbols), with Bax only (open circles), or with tBid only (open squares). (C) Percentage of ANTS release after 2 h as a function of r. The open crosses represent data obtained at low lipid concentration (0.04 g/l or 50 μM, average ± stdev, n = 3), while the open squares represent data obtained at high lipid concentration (7.3 g/l or 9.5 mM, n = 1). The empty circles represent data obtained with DiD-labeled liposomes in one experiment in order to ensure that relative Bax-to-liposome ratios were exact even when using liposomes of different sizes. The filled circles represent data obtained for EGFP-Bax. (D) Same data as in (C), plotted as a function of P/L. (E) Percentage of ANTS release after 2 h as a function of Bax concentration for different lipid concentrations (50 nm diameter liposomes). Lines represent exponential fit to the data according to Eq. (6). (F) $P^*(L)$, as a function of lipid concentration, as obtained from the fits shown in (E). Line is a linear fit to the data, which gave a = 57 nM and b = 4.8 nM/μM.

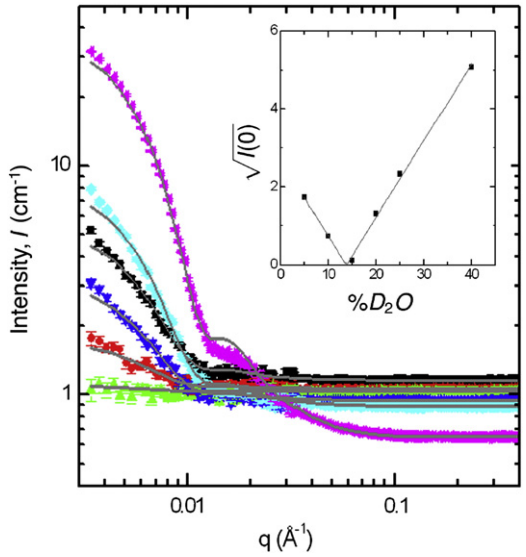

Fig. 6. Neutron scattering of liposomes as a function of % D_2O. Scattered intensity as a function of scattering vector obtained for liposomes with a mitochondria-like lipid composition in buffer containing different percentages of D_2O (black squares: 5% D_2O, red circles: 10% D_2O, green triangles: 15% D_2O, inverted dark blue triangles: 20% D_2O, light blue diamonds: 25% D_2O, pink sideway triangles: 40% D_2O). Gray lines are fits to the data using the one-strip shell model. Note that the background level increases with the increasing content of H_2O as a result of incoherent scattering from hydrogen. Inset: Square-root zero angle intensity of the scattering as a function of % D_2O.

Finally, we used the ANTS release data measured for 50 nm diameter liposomes at three different lipid concentrations (Fig. 5E) to obtain an estimate of the equilibrium constant describing Bax binding to the lipids, following an approach previously used to measure the membrane binding constant of a pore forming peptide [58]. The ANTS release data was fit assuming an exponential dependence on Bax concentration (Eq. (6)), providing three different values for the parameter P^*, which showed a linear dependence on L (Fig. 5F), as expected for a simple equilibrium (see Section 2.7.2 in Materials and methods for details). This provided an estimate of the apparent binding constant of Bax to lipid membranes, $K = 0.084\ \mu M^{-1}$. Although this value is at least one order of magnitude lower than those obtained from the FIDA experiments presented in the previous section, one needs to consider that this corresponds to an effective Bax binding constant before the samples have been passed through the size-exclusion column, that is before any inactive protein is eliminated from the sample (and indeed samples examined by FIDA before the size-exclusion column showed lower Bax binding levels).

3.6. Contrast matching of mitochondrial-like liposomes

Liposomes used in this study were made from a mix of lipids (PC, PE, PI, PS and CL) reflecting the lipid composition of mitochondrial membranes. To verify that good neutron contrast matching could be obtained for these membranes, a series of SANS experiments was performed for liposomes in buffer containing between 5% and 40% D_2O, at a constant lipid concentration of 5.3 g/l. Scattered intensities (I) plotted as a function of scattering vector (q) are shown in Fig. 6. The intensity of the scattering curves, $I(0)$, is related to the square of the contrast between the average SLD of the lipid membrane, SLD_S, and the SLD of the buffer, SLD_W, i.e., $I_{S+W}(0) \propto (SLD_S - SLD_W)^2$ [65]. One then expects $\sqrt{I(0)}$ to be linear as a percent of D_2O in the buffer. In determining $I(0)$, by fitting the scattering curves with the one-strip shell model and plotting $\sqrt{I(0)}$ as a function of % D_2O (Fig. 6, inset), a linear dependence was observed with a contrast match point at 15% D_2O.

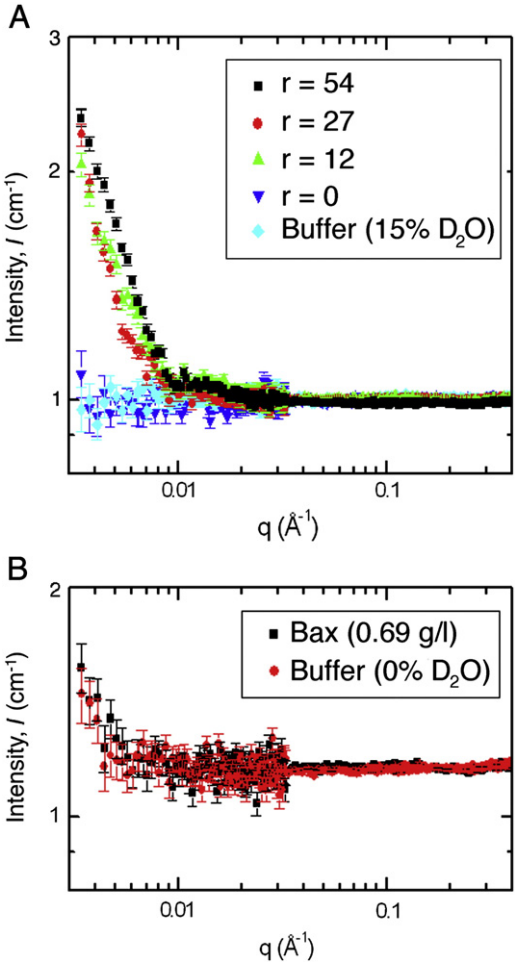

Fig. 7. Neutron scattering of liposomes with Bax and tBid at 15% D_2O. (A) Scattering data obtained for Bax and tBid incubated with liposomes at the lipid contrast match point (15% D_2O), compared to the data obtained for liposomes alone and buffer alone (also at 15% D_2O). (B) Scattering data obtained for soluble monomeric Bax (0.69 g/l or 31 μM) compared to scattering from the buffer at 0% D_2O.

3.7. Membrane associated Bax can be detected by SANS

SANS data for Bax incubated with liposomes and activated by tBid was recorded in 15% D_2O buffer (that is at the lipid membrane contrast match point, when only scattering from the proteins should be recorded) at high Bax-to-liposome ratios (estimated r = 12, 27 and 54, obtained using protein and lipid concentrations as listed in Table 1), that is in the limit where binding of Bax to the liposomes is saturated. The corresponding scattered neutron intensities are shown in Fig. 7A, where they are compared to SANS scattering curves obtained from liposomes in the absence of protein (r = 0, lipid concentration of 7.33 g/l). As expected, no scattering was observed for the sample containing only lipids (r = 0), since 15% D_2O corresponds to the membrane contrast match point. On the other hand, a clear scattering signal was observed when proteins were present, and this was true for all Bax-to-liposome ratios explored. To check whether part of this signal might correspond to scattering as a result of untargeted monomeric Bax in solution, the scattering by soluble monomeric Bax (in the absence of liposomes) was measured in 0% D_2O (Fig. 7B). The contrast between protein and buffer is larger at 0% D_2O than at 15% D_2O, and the Bax concentration used in this control experiment (0.69 g/l) was higher than the total Bax plus tBid protein concentration in either of the membrane-inserted Bax samples studied (which varied between 0.31 and 0.61 g/l, see Table 1). Despite this, no scattering was observed showing that soluble monomeric Bax does not significantly scatter

neutrons under the experimental conditions used for this study. This was expected given the small radius of gyration of soluble Bax (~2 nm), and assuming no long-range correlations between its monomers. Over the *q* range studied, soluble Bax would give rise to a constant incoherent scattering (i.e. background), and the diffuse scattering produced by individual Bax molecules would not be observed (whereas we expect to detect scattering from membrane bound Bax species which reside on the membrane of larger objects – liposomes – and may also be part of large oligomers). This conclusion also applies to soluble tBid (although no significant amount of tBid is expected to be present in solution), since tBid has a lower molecular mass than Bax, and is only present in low concentrations (0.037 to 0.073 g/l). Thus the scattering signal observed for 15% D_2O liposomes containing activated Bax can only be attributed to proteins bound to liposomes.

3.8. Distribution of Bax on liposomes

In order to better observe the distribution of the protein with respect to the lipid membrane, contrast variation experiments were performed where the buffer's SLD was systematically varied. Contrast variation (i.e. altering the D_2O content of the buffer) does not alter the system under study, but allows rendering parts of this system (e.g. the lipids at 15% D_2O and the proteins at 40% D_2O) "invisible" to the neutrons, and thus obtaining structural information about the rest of the system (e.g. the proteins at 15% D_2O and the lipids at 40% D_2O) separately. For each of the three Bax-to-liposome ratios investigated (estimated r = 12, 27, and 54), as well as for a control sample with liposomes in the absence of proteins (r = 0), SANS data were collected at 15%, 40% and 60% D_2O. The data obtained for r = 54 in different buffer conditions is shown in Fig. 8A (allowing in particular to directly compare the scattering from the membrane bound proteins, at 15% D_2O, and the scattering from the lipids, at 40% D_2O). The data obtained at 40% D_2O for all Bax-to-liposome ratios explored is shown in Fig. 8B (allowing to directly compare the scattering from the lipids in the presence of different amount of proteins). One striking feature of the data was that for different contrast conditions scattering curves were very similar (e.g., Fig. 8A), except that at 15% D_2O the amount of signal was much lower (as expected since at 15% D_2O only the few proteins present contribute to the neutron scattering signal), and the amount of background much higher (as expected due to increased incoherent scattering from H_2O). This similarity between the different contrast conditions does not mean that lipids still scatter at 15% D_2O (since we have shown in the previous section that this was not the case), but rather can be understood if one assumes that there were at least two independent scattering units per liposome, either protein monomers or protein oligomers.

Two or more protein scattering centers constrained within the surface of the same liposome would result in interferences between neutrons scattered by these different proteins, giving rise to intravesicular pair interference terms in the scattering function. Taking into account the independent relative orientations of these scattering centers on different liposomes, this translates in the object being best described by a spherical shell with a radius similar to that of a liposome, as illustrated in Fig. 9. In this case, the scattering data obtained from the protein on the liposomes (i.e. the data obtained at 15% D_2O) is expected to resemble the scattering data obtained from the liposomes themselves (i.e. the data obtained at 40% D_2O). Consequently, the scattering curves obtained in the presence and in the absence of protein were analyzed using either the one-strip or the asymmetric two-strip model, as described in the Materials and methods section. First, the three scattering curves obtained at a given contrast matching condition for all three samples with proteins (r = 12, 27 and 54) were considered as an ensemble. At 40% D_2O (the contrast match point of the protein), both the individual and global analysis of the data with the one-strip model indicated that the hydrophobic part of the lipid bilayer formed a shell with an average radius of 28.1 ± 0.1 nm and a thickness of 3.2 ± 0.1 nm, i.e., the inner radius of the liposome is ~26 nm and the outer

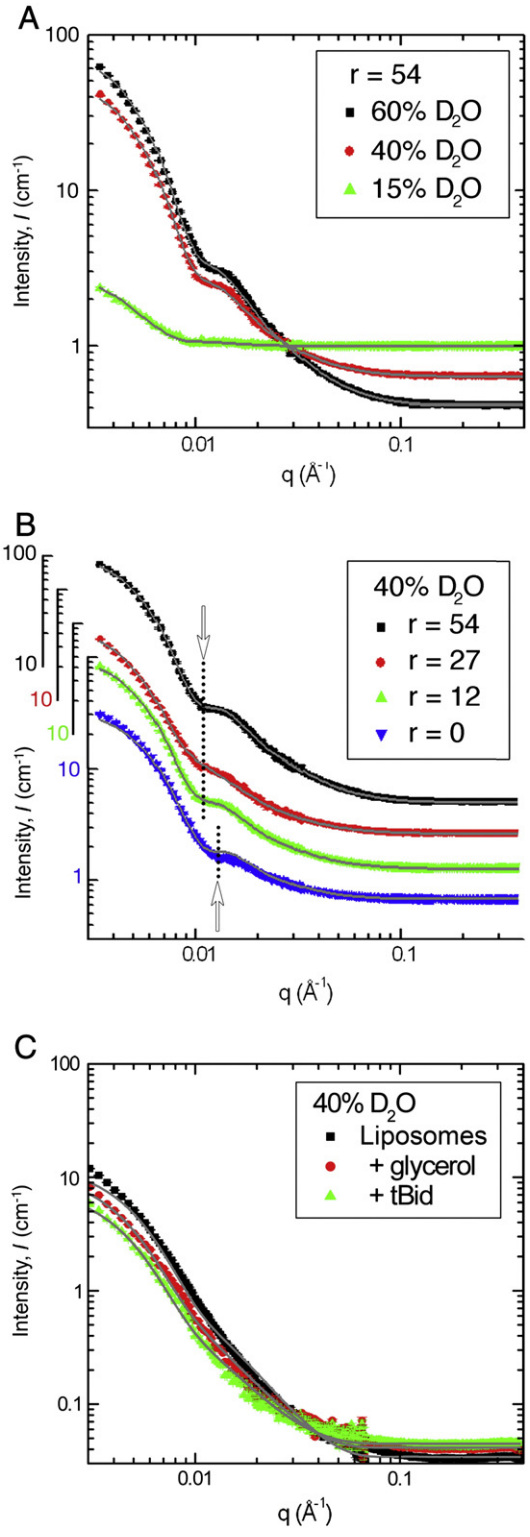

Fig. 8. Neutron scattering of liposomes with Bax and tBid for different contrast conditions. (A) Scattering curves obtained for a Bax-to-liposome ratio r = 54 under different contrast conditions. Solid lines are fits to the data using the asymmetrical two-strip model. Note that the background level increases with the increasing content of H_2O, because of the incoherent scattering from hydrogen. (B) Scattering curves obtained at the protein contrast match point (40% D_2O) for liposomes in the absence of proteins and for three different Bax-to-liposome ratios. Solid lines are fits to the data using the one-strip model. Arrows and dotted lines indicate the approximate position of the first minimum of the scattering curves. Curves have been shifted vertically for clarity. (C) Scattering curves obtained at the protein contrast match point (40% D_2O) for liposomes in buffer, liposomes in buffer with glycerol, and liposomes with tBid in buffer with glycerol. Data shown in (C) were obtained using the ORNL SANS instrument.

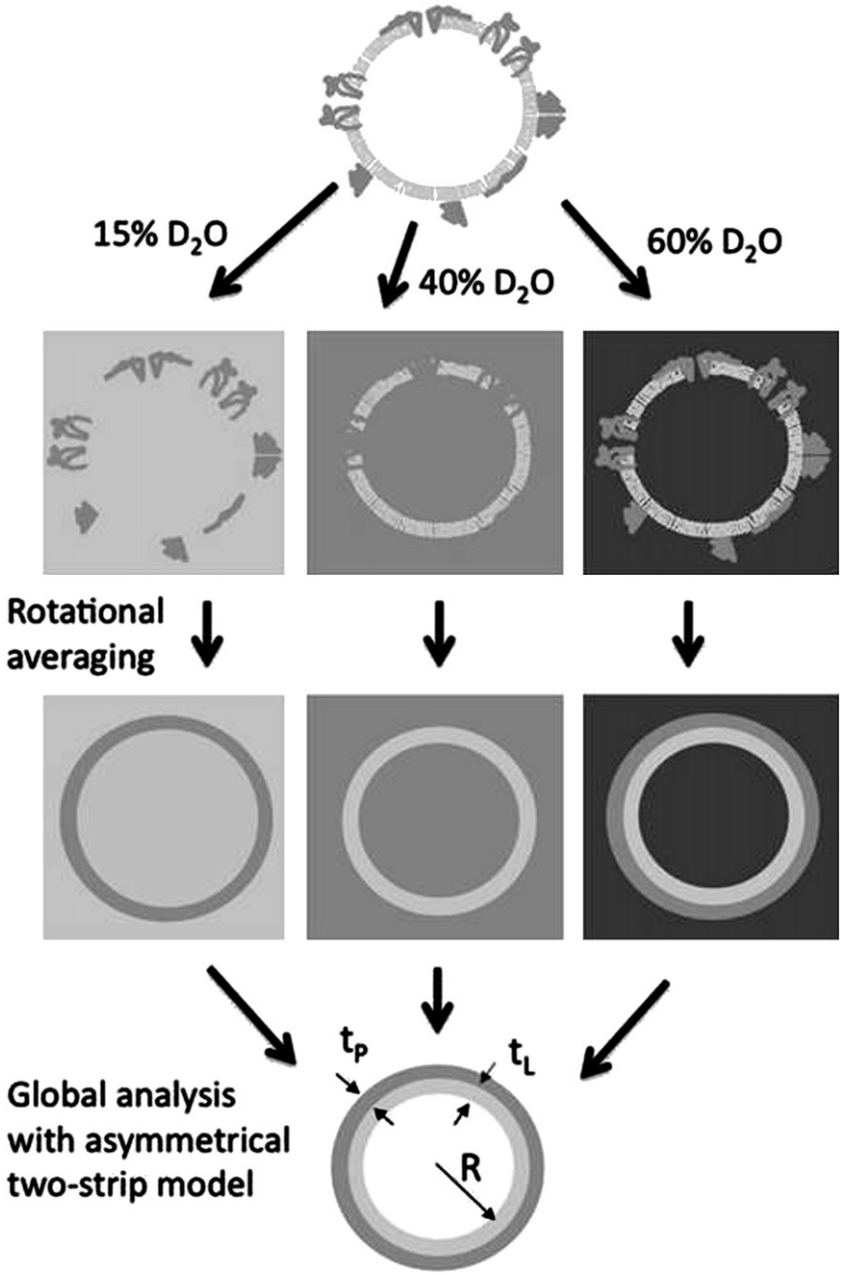

Fig. 9. Schematic of the neutron contrast variation experiment. For a liposome with Bax inserted in its membrane (top row, with Bax represented in a variety of possible conformations), the diagram represents the principle of the neutron contrast variation experiment (second row), the rotational averaging brought about by SANS (third row), and the result of the global analysis using the asymmetrical two-strip model (fourth row).

radius is ~30 nm. In parallel, at 15% D_2O (the contrast match point of the lipids), both the individual and global data analysis with the same one-strip model indicated that the thickness of the protein shell was 11 ± 1 nm, with an average radius of 30.4 ± 0.6 nm, meaning that the proteins were positioned between ~25 nm (inner radius) and 35 nm (outer radius) from the center of the liposome. From this simple analysis, it is evident that the protein forms a significantly thicker layer than the lipid bilayer, with most of the protein mass protruding beyond the lipids, on the outside of the liposomes.

A slightly more refined approach consisted in performing a global fit to the scattering data obtained for a given Bax-to-liposome ratio at different contrast match points, allowing for the use of the asymmetric two-strip model. Results from this analysis are summarized in Table 1. At all Bax-to-liposome ratios explored, the picture was essentially the same as that from the simple one-strip model. The radius of the liposomes was on average R ~27.5 nm, the hydrophobic part of the lipid bilayer had a thickness t_L of ~3.3 nm, and the protein layer residing above the lipid bilayer had a thickness t_P of ~5 nm. This last feature was present at all protein-to-liposome ratios, however, protein thickness was obtained reliably only at r = 54, for which the signal-to-noise ratio was more favorable than for the other samples. Protein thickness was then constrained when analyzing the data obtained for r = 27 and r = 12 samples.

3.9. Changes to the lipid bilayer upon interaction with tBid-activated Bax

An interesting aspect of the interaction between a protein and a lipid membrane is the influence that the protein will have on lipid

organization. Modifications to the lipid bilayer can be assessed by comparing the scattering curves obtained at the protein contrast matching point (40% D_2O), in the presence and in the absence of protein (Fig. 8B). Analyzing these data with the one-strip model, where the strip represents the hydrophobic part of the lipid bilayer, allows one to determine how the presence of the proteins influences the radius and thickness of the lipid shell. In the presence of tBid-activated Bax proteins, two very clear effects were observed. First, the radius of the liposomes increased by about 18%, from 23.7 nm in the absence of protein to ~28 nm in the presence of Bax with no visible dependence on the amount of Bax for r = 12 to 54 (in Fig. 8B this increase is reflected in the shift of the first minimum of the scattering curves towards lower q in the presence of protein). This radius increase corresponds to a ~40% increase in the liposome's surface area, i.e. the surface of each liposome increased by ~2800 nm^2. Second, the membrane's hydrophobic thickness decreased by ~11%, from 3.8 nm in the absence of protein to ~3.4 nm in the presence of protein, again with very little dependence on the Bax-to-liposome ratio under the conditions explored here. These results are in agreement with those obtained from the global fit of the data obtained at different D_2O concentrations using the two-strip model (Table 1). In particular, the increase in liposome radius is a robust observation, and although liposomes used in the different SANS experiments came from several different batches, liposome radius was very reproducible from one batch to another.

In a separate series of SANS experiments, it was verified that the observed membrane thinning was not due to the action of tBid or to the presence of glycerol (since in the samples used for the SANS experiments used above, the presence of Bax was correlated with that of glycerol, see Table 1). In order to do so, liposomes were incubated in 40% D_2O buffer either 1) on their own, 2) with glycerol alone or 3) with glycerol and tBid, and SANS scattering curves were recorded. The lipid concentration (4.8 g/l), glycerol concentration (5.4%) and tBid concentration (0.04 g/l) used for these experiments were comparable to those used in the experiments presented in Fig. 8B (for which the lipid concentrations were 10.9 g/l, 4.8 g/l and 4.8 g/l, the glycerol concentrations were 5.2%, 5.3% and 6% and the tBid concentrations were 0.024 g/l, 0.024 g/l and 0.048 g/l, for r = 12, 27 and 54, respectively). Liposomes in all three samples came from the same batch. Although the resolution of these experiments was lower than that obtained in previous SANS experiments, analysis with the one-strip model convincingly showed that the radius of the liposomes was unaffected by the presence of either glycerol or tBid, remaining at r = 22 +/− 0.6 nm for all three samples measured. Therefore the observed membrane thinning is specifically due to the interaction of Bax with the membrane.

4. Discussion

4.1. Models for analyzing SANS data

Neutron scattering represents a unique opportunity for the investigation of membrane protein oligomers because of the possibility of studying the system at the contrast match point of either the lipid or the protein [44]. Here we used a 50 nm diameter liposomal system, which mimics the mitochondrial membrane and its interactions with proteins as argued below. In describing the system, the data were analyzed using either a one-strip hollow sphere model (for liposomes alone, or for liposomes with proteins at either the contrast match point of the protein or the liposomes) or a two-strip hollow sphere model (for liposomes in the presence of proteins), which was sufficient to adequately fit the data. Despite the simplicity of these models, features such as liposome radius, membrane thickness, and protein thickness are well and robustly resolved. In addition, the mere fact that the protein signal (i.e. liposomes with proteins at the contrast match point of the lipids) could be fitted with the hollow sphere model resulted in important information regarding the protein's distribution on the liposome's surface.

4.2. Interaction of Bax with small diameter liposomes at high Bax-to-lipid ratios

Gel-filtration experiments followed by immunoblotting and fluorescence experiments confirmed that tBid-activated Bax binds to 50 nm diameter biomimetic mitochondrial membranes, forms oligomers when interacting with them and is able to permeabilize them, with the amount of permeabilized liposomes becoming significant for Bax-to-liposome ratios larger than ~10. The data collected in this study show that at a given protein-to-lipid ratio (a quantity whose relative values could be controlled very precisely using fluorescently labeled proteins and liposomes), the amount of Bax binding, Bax oligomerization and Bax-mediated liposome permeabilization were comparable for 50 nm diameter liposomes, 100 nm liposomes (a size of liposome often used in in vitro studies of Bcl-2 family proteins [14,17,50]) and 200 nm liposomes. As a matter of fact, the apparent association constant measured for Bax binding to 50 nm diameter liposomes is ~2-fold larger than that measured for 100 nm liposomes ($K = 3\ \mu M^{-1}$ in the first case and $K = 1.3\ \mu M^{-1}$ in the second case). These observations are in contrast to a previous report that liposomes smaller than 200 nm in diameter barely support Bax binding and do not support Bax oligomerization [66]. However, the lipid composition used in our study, which approximates the lipid composition of mitochondrial membranes, was different from the lipid composition used in Ref. [66] (which contained no PS, but instead contained cholesterol). In addition, the Bax protein used in Ref. [66] still had a Histidine tag, whereas the Bax proteins used in our study did not. One should also note that although it has been shown that Bax permeabilization is enhanced in the presence of lipids with positive intrinsic curvature such as PS, this does not mean that the curvature of the lipid bilayer (and therefore the size of the liposomes) influences Bax interaction with membranes. Rather, it suggests that the Bax pore structure is lipidic and that the curvature of the lipid monolayer at the pore is highly positive [14].

Although Bax binding was discussed here in terms of a simple equilibrium between soluble Bax and membrane associated Bax, the actual experimental system obviously has several more layers of complexity: 1/the activation process by tBid – which was rendered inconspicuous here since tBid was mostly always present in excess – obviously plays essential role for Bax binding, 2/the distribution of Bax on the liposomes is not likely to be random at small protein-to-lipid ratios, as it has been shown that a truncated autoactive version of Bax was forming pores in a cooperative manner [12], 3/inactive Bax proteins or Bax proteins binding to the sample surfaces might displace the equilibrium, and 4/Bax may have several membrane-bound conformations, as further discussed below. It is then all the more striking that for a given liposome size the fraction of bound Bax primarily depends only on protein-to-lipid ratio. The simple partition model predicts that the percentage of bound Bax (Eq. (3)) and the number of bound Bax per liposome (Eq. (5)) should depend on Bax concentration as well as on protein-to-lipid ratio. Yet, when the binding data shown in Fig. 3B was subdivided according to Bax concentration, only a weak dependence on P was found, where the value obtained for KP (by fitting the data with the simple equilibrium model) increased less than 2-fold for a 10-fold increase in P. This means that membrane binding becomes weaker when Bax concentration is increased. As a result, the amount of bound Bax does not strongly depend on Bax concentration. For tBid concentrations higher than ~1 tBid per liposome, neither does it depend on tBid concentration. Instead the amount of bound Bax (and in particular the maximum amount of Bax molecules per liposome reached at high Bax concentration) primarily depends on the Bax-to-liposome ratio. This suggests that Bax binding is critically regulated by some property of the lipid membrane, for example lipid composition (i.e. the presence of a particular lipid receptor), membrane charge, or membrane tension. It must also to some extent be regulated by membrane curvature, since as mentioned above the apparent binding constant describing the

interaction between Bax and lipids is slightly dependent on liposome size, however this effect seems weak. Importantly, this weak dependence of binding on Bax concentration explains the saturation of the number of bound Bax per liposome observed in our system. The partition models predict that at low liposome concentrations ($L \ll 1/K$, which was the case in the fluorescence experiments presented here) Bax binding should saturate when L decreases and P/L increases, reaching the limit value $n = mKP$ (Eq. (5)). Given the values estimated for KP from the measured binding isotherm (Fig. 3B), this indeed corresponds to a limit value of $n \approx 10$ for 50 nm diameter liposomes. It is possible that this limit value will slightly increase with increasing protein and lipid concentration, and it therefore constitutes a lower bound for the number of Bax proteins in high protein and lipid concentrations samples used here for SANS.

Importantly, all of the observations made highlighted the system's robustness. The insertion of tBid and Bax into the membrane has been suggested to result in destabilization of lipid bilayers in vitro [67,68], and Bax has been observed to participate into mitochondrial remodeling during apoptosis in vivo [69,70]. However, even at high lipid concentrations (up to 17 g/l or 22 mM) and high Bax and tBid concentrations (up to 24.5 μM for Bax and 4.9 μM for tBid), the average dimension and polydispersity of the liposomes remained constant over periods of more than 24 h (the duration of a scattering experiment), an observation consistent with the fact that the size and specific brightness of liposomes (as measured by FCS and FIDA) was never observed to change over time in our experiments, whatever the concentration of Bax and tBid added. This shows that destabilization upon addition of tBid and Bax, if present, does not result in deformation, breaking up, fusion or aggregation of the liposomes, that is to say the membrane openings formed by Bax do not perturb the structure of the liposomes on the macroscopic scale. This is consistent with previous observations in which incubation of outer mitochondrial membrane liposomes with Bax and cleaved Bid resulted in the release of 2000 kDa dextran molecules, but with no detectable morphological changes in the structure of liposomes, as assessed by electron microscopy [15]. In addition, the fact that the scattering data could be well fit by the asymmetric two-strip model indicates that the bulk of the protein remained on the outside surface of the liposomes. In other words, even after 24 h the proteins have not significantly penetrated the liposomal membrane. Instead, they have remained bound or inserted in the membrane in the same orientation as when they were first introduced. Thus, although Bax pore formation induces the exchange of lipids between the two membrane leaflets [21], it does not promote flip-flop of the proteins themselves, or at least not for a significant fraction of the bound proteins.

In conclusion, all the data collected point to the viability of the present model system, which contained high lipid concentrations under the form of small liposomes and high activated Bax-to-liposome ratios ($r > 10$), as a mimic for a pore-forming protein in a lipid membrane.

4.3. Membrane conformations of Bax

Whereas the conformation of Bax in membranes remains unknown – apart from the fact that in its active form helices 5, 6 and 9 are inserted into the lipid bilayer – the membrane conformations of anti-apoptotic Bcl-XL and tBid have been the object of numerous structural investigations. The results of a solid state NMR study of Bcl-XL inserted in a synthetic membrane were consistent with a model where most of the α-helices of the protein were arranged parallel to the membrane, while a few other helices were arranged at some angle from the plane of the membrane (presumably helices 5 and 6) [71]. This type of "umbrella conformation" was first described for bacterial colicins [72]. In the case of tBid, NMR [73], spin labeling [74], and Monte Carlo simulations [75] concur that all six helices are arranged more or less parallel to the plane of the membrane. This led to the proposition that Bax would also adopt an "umbrella" conformation with helices 2, 3, 4, 7 and 8 arranged parallel to the membrane, and further, that an intermediate conformation of Bax may be present where all of its helices would lay parallel to the membrane [41]. However, membrane inserted Bax differs from membrane bound Bcl-XL and tBid in important ways, namely in its capacity to oligomerize and to permeabilize membranes.

The SANS data presented in this study unequivocally shows that for lipid membranes exposed to tBid-activated Bax, a ~5 nm thick protein layer is present in places above the lipid bilayer. Analysis of the data obtained at 15% D_2O and 40% D_2O using the one-strip model shows that the protein layer is thicker than the lipid layer, and for data obtained at 60% D_2O the two-strip model gives a significantly better fit than the one-strip model. This emphasizes the importance of membrane bound Bax conformations for which most of the protein is protruding above the membrane, and invalidates the possibility that all membrane conformations of Bax are umbrella-like. According to our targeting and permeabilization assays, under the conditions explored in our SANS experiments (estimated $r \geq 12$) at least 10 Bax proteins were bound to each liposome (Fig. 3) and at least some of these proteins were in their pore-forming conformation – since most liposomes were permeabilized (Fig. 5). Therefore, one possible interpretation of the SANS data is that the protein coat detected corresponds to a cap formed by Bax pores. An atomic force microscopy study of supported lipid bilayers hinted at this possibility by showing that in the presence of Bax, small pores were surrounded by a rim approximately 5 nm high [22]. This could occur if membrane-inserted Bax adopts a mushroom conformation (e.g. such as conformation C represented in Fig. 1), or if Bax molecules peripherally bind to either Bax or tBid proteins lining the pores (conformation similar to B in Fig. 1). Mushroom conformations have been observed for several other pore-forming proteins, in particular for the staphylococcal toxin α-hemolysin [76]. However, this protein forms stable proteinaceous pores very different in nature from the variable size lipidic pores formed by Bax [12,16,21].

A second possible interpretation of the data is that the conspicuous protein layer observed above the membrane corresponds to proteins peripherally bound to the liposomes (resembling conformation B in Fig. 1, where the overall soluble structure of the protein is conserved and no helices are inserted in the membrane). The idea that Bax may have a peripheral, loosely bound conformation, is consistent with the observation made in several previous studies that in its non-activated state Bax weakly and transiently interacts with lipid membranes. First, in vitro, Bax changes conformation (exposing the 6A7 isotope) in the sole presence of membranes [17]. Since our own observations show that in these conditions Bax does not lastingly bind to liposomal membranes, it means that it must transiently interact with them. Second, in healthy cells a small fraction of Bax is found attached to mitochondria, yet this fraction is carbonate-extractable, meaning that the interaction between the Bax molecules and the membrane is weak [10,32]. Finally a recent study has shown that Bax constantly shuttles from the cytoplasm to the mitochondria, showing that this weak interaction is also transient [77]. Although this weak interaction between Bax and lipid membranes is short lived in the absence of tBid, it could be that tBid stabilizes Bax's peripherally bound conformation. If a significant fraction of peripherally bound Bax is present, this conformation is stable enough that it remains present on the membrane after gel-filtration – our fluorescence experiment before gel filtration shows the same percentage of bound Bax as the gel-filtration analysis. Peripherally bound proteins, even in a monomeric state, would have contributed to the SANS signal, as they would have been part of a larger scattering unit (i.e. liposomes with several peripherally bound proteins). The observed thickness of the protein layer, ~5 nm, is consistent with the presence of Bax proteins only weakly interacting with the membrane and adopting a conformation similar to their solution conformation, since the diameter of soluble Bax is ~4 nm (as inferred from its NMR structure, PDB ID: 1F16) [27]. The existence of peripherally bound Bax in a compact conformation, such as conformation B in Fig. 1, is also supported by Monte Carlo simulations [78]. Although

in this scenario there would then be no evidence of a membrane inserted Bax conformation in the SANS data, such a conformation (e.g. an umbrella-like conformation such as conformation E in Fig. 1) would be very difficult to detect in the presence of a more conspicuous peripheral compact conformation. Thus the fact that it was not observed does not mean that it does not exist.

If indeed Bax adopts several different conformations at the membrane, as suggested in this second scenario, then the binding isotherm shown in Fig. 3B suggests that all these conformations are in equilibrium, and are also in equilibrium with soluble Bax. Therefore the transition between loosely bound and membrane-inserted Bax must be reversible, and the pores must have a transient rather than stable structure. The idea that different Bax states are in equilibrium is supported by several previous observations, in particular the observation that the Bax-Bax interactions in Bax oligomers can be displaced by new Bax [50], and the observation that Bax constantly shuttles from cytoplasm to membrane in healthy cells [77]. Likely, the relative amount of different Bax conformations is influenced by a number of parameters. In particular, it is conceivable that the prominence of peripherally bound proteins is increased for small liposomes.

4.4. Distribution of Bax proteins on liposomes

At all Bax-to-liposome ratios studied by SANS, the protein scattering data contained an intra-vesicular pair interference term (i.e. a term arising from the presence of several protein scattering units on the surface of the same liposome), which betrayed the presence of at least, on average, two independent protein units (monomer or oligomer) associated with each liposome [44]. According to our membrane targeting assay, under these conditions (estimated r = 12 or larger) each liposome has at least on average ~10–15 Bax proteins and ~2 tBid proteins either inserted in or peripherally associated with its membrane, forming at least one pore in at least 50% of the liposomes. In vitro studies of the kinetics of dye release from liposomes performed with a truncated version of Bax led to the conclusion that Bax was forming dimers and tetramers in lipid membranes [12]. Our observation that Bax is distributed over the surface of the liposome is consistent with the presence of small pores, as observed by Saito et al. for the truncated protein [12]. It is very likely, however, that the SANS signal detected comes at least in part from peripherally bound and potentially monomeric Bax.

Whether the SANS signal detected comes from inserted Bax, peripherally bound Bax, or both, the observed distribution of Bax on the membrane of the liposomes is in sharp contrast to that observed in a previous SANS study for the pore-forming protein pneumolysin [46]. In the case of pneumolysin, no intra-vesicular pair interference term was observed, and it was shown that the protein formed a single toroidal oligomeric structure [46]. Pneumolysin, like α-hemolysin, belongs to a class of pore-forming proteins (PFPs) known as β-PFPs whose membrane insertion domain becomes part of a β-sheet structure when inserted in the membrane [79]. Bax, on the other hand, is classified as an α-PFP along with other proteins, such as the diphtheria toxin and colicins, for which the main motif of the pore-forming domain is an α-helical hairpin. In broad terms, whereas β-PFPs tend to form stable barrel-stave pores with a well-defined stoichiometry, α-PFPs tend to form unstable toroidal pores with variable stoichiometries. This difference seems reflected here in the distribution of Bax proteins into several scattering centers distributed over the surface of each liposome, as opposed to the organization of the pneumolysins proteins, which form one single stable pore. It points to a mechanism of action of Bax on the membrane that could be global rather than or as well as local, i.e. where the influence of Bax on global membrane properties such as surface tension is at least as important as the local creation or pores on the membrane.

4.5. Effect of Bax insertion in the membrane of liposomes

Membrane thinning and surface area expansion are well documented consequences of the insertion of antimicrobial peptides into lipid membranes [80–82] and have also been observed after the insertion of pneumolysin in liposomal membranes [46], but have yet to be reported for any full-length Bcl-2 family protein. In the case of antimicrobial peptides, a strong body of evidence indicates that membrane thinning is caused by peptides inserting parallel to the plane of the membrane, between lipid headgroups, thereby forcing the hydrophobic chains to reorganize with their carbonyl chains at an angle with the bilayer normal. This causes a tension in the membrane which, above a certain threshold peptide-to-lipid ratio, prevents the insertion of additional peptides parallel to the membrane and further membrane thinning, and instead promotes the insertion of peptides perpendicular to the plane of the bilayer and the formation of pores [83]. The observed threshold peptide-to-lipid ratio for peptide insertion and pore formation varies from ~1:10 to less than 1:200 depending on the peptide [80].

Our observation that the binding of full-length Bax to liposomal membranes causes membrane thinning suggests that the pore formation mechanism exhibited by proteins of the Bcl-2 family resembles that of antimicrobial peptides, i.e. for which the driving force is the induction of membrane tension through surface thinning. Such a mechanistic link has already been considered on theoretical grounds [84] and is supported by previous observations of a structural link between the pores formed by Bax [14,16,21] or Bax-derived peptides [38], and the pores formed by antimicrobial peptides – namely that both types of pores are lipidic. By analogy with the case of pore-forming peptides, we thus expect that for a threshold value of P/L membrane pores will form in the membrane of liposomes, and that this threshold value also corresponds to the P/L at which membrane thinning reaches its limit value. Strikingly, we did observe that for liposomes of different sizes pore formation occurs at the same P/L (when a pore formation not relying on surface tension would predict that pore formation would instead occur at a given r), with a threshold value around P/L ~1:2000, that is at an α-helix-to-lipid ratio around ~1:200, in agreement with what is observed for pore-forming peptides. Since all the SANS experiments presented here were performed above this threshold value, we do not expect to observe any further variation in membrane thickness with Bax concentration. Indeed, the ~10% decrease in membrane thickness that we observe for $r \geq 12$ upon interaction with Bax is independent of Bax concentration, and is on the order of the maximum thinning observed for different pore forming peptides above the threshold concentration for pore formation [84]. It is also significant to note that in the conditions of our experiments, tBid (which on its own does not cause membrane permeabilization) did not cause membrane thinning, reinforcing the idea that membrane thinning is closely linked to membrane permeabilization.

Membrane deformation by Bax also raises the possibility of long-range interactions between proteins mediated by the membrane. Particles inducing either membrane thinning or membrane curvature interact with each other because their relative position can affect the elastic properties of the membrane [85,86]. The fact that Bax causes strong membrane thinning might help explain the tendency of this protein to homo-oligomerize when inserted in a lipid membrane, to act as a receptor for itself [87], or even to interact with other membrane inserted Bcl-2 family proteins. It is known that lipid bilayers have a great influence on protein–protein interactions between Bcl-2 family members. However, the mechanism by which the lipids control these interactions remains unknown [3,88,89]. Our work suggests a possible explanation where these interactions are in part induced by membrane deformations.

5. Conclusion

The major findings of this study of Bax interaction with liposomes are: a) In the presence of excess tBid, Bax binding to 50 nm diameter

liposomes is well described by an equilibrium with an apparent association constant $K \approx 3\,\mu M^{-1}$, resulting at high Bax-to-liposome ratios in at least 10 Bax molecules per liposome; b) These molecules are not localized in a single oligomer, but rather are distributed over the surface of the liposome; c) Most of these Bax molecules are not fully incorporated into the membrane, but rather protrudes significantly from the membrane; d) Bax causes the membrane to thin, an effect which is accompanied by an increase in liposome radius. Although well-established for pore-forming peptides, this is the first time that anyone has reported membrane thinning for any full length Bcl-2 family protein.

Acknowledgements

We thank Dr. Boualem Hammouda for help on the NG3 beamline at NIST, and Dr. William Heller for help on the Bio-SANS instrument at ORNL. This work was funded by the Canadian Institutes of Health Research (CIHR), grant FRN-86657. C.F. is the recipient of a Canada Research Chair funded by the Natural Sciences and Engineering Research Council (NSERC). D.W.A. is the recipient of a Tier 1 Canada Research Chair funded by the CIHR.

References

[1] C. Twomey, J.V. McCarthy, Pathways of apoptosis and importance in development, J. Cell. Mol. Med. 9 (2005) 345–359.
[2] N.N. Danial, S.J. Korsmeyer, Cell death: critical control points, Cell 116 (2004) 205–219.
[3] B. Leber, J. Lin, D.W. Andrews, Embedded together: the life and death consequences of interaction of the Bcl-2 family with membranes, Apoptosis 12 (2007) 897–911.
[4] S. Cory, D.C. Huang, J.M. Adams, The Bcl-2 family: roles in cell survival and oncogenesis, Oncogene 22 (2003) 8590–8607.
[5] R.J. Youle, A. Strasser, The BCL-2 protein family: opposing activities that mediate cell death, Nat. Rev. Mol. Cell Biol. 9 (2008) 47–59.
[6] J.M. Jurgensmeier, Z. Xie, Q. Deveraux, L. Ellerby, D. Bredesen, J.C. Reed, Bax directly induces release of cytochrome c from isolated mitochondria, Proc. Natl. Acad. Sci. U. S. A. 95 (1998) 4997–5002.
[7] S. Desagher, A. Osen-Sand, A. Nichols, R. Eskes, S. Montessuit, S. Lauper, K. Maundrell, B. Antonsson, J.C. Martinou, Bid-induced conformational change of Bax is responsible for mitochondrial cytochrome c release during apoptosis, J. Cell Biol. 144 (1999) 891–901.
[8] K.G. Wolter, Y.-T. Hsu, C.L. Smith, A. Nechushtan, X.-G. Xi, R.J. Youle, Movement of Bax from the cytosol to mitochondria during apoptosis, J. Cell Biol. 139 (1997) 1281–1292.
[9] Y.T. Hsu, K.G. Wolter, R.J. Youle, Cytosol-to-membrane redistribution of Bax and Bcl-X(L) during apoptosis, Proc. Natl. Acad. Sci. U. S. A. 94 (1997) 3668–3672.
[10] B. Antonsson, S. Montessuit, B. Sanchez, J.C. Martinou, Bax is present as a high molecular weight oligomer/complex in the mitochondrial membrane of apoptotic cells, J. Biol. Chem. 276 (2001) 11615–11623.
[11] A. Gross, J. Jockel, M.C. Wei, S.J. Korsmeyer, Enforced dimerization of BAX results in its translocation, mitochondrial dysfunction and apoptosis, EMBO J. 17 (1998) 3878–3885.
[12] M. Saito, S.J. Korsmeyer, P.H. Schlesinger, BAX-dependent transport of cytochrome c reconstituted in pure liposomes, Nat. Cell Biol. 2 (2000) 553–555.
[13] R.F. Epand, J.C. Martinou, S. Montessuit, R.M. Epand, Membrane perturbations induced by the apoptotic Bax protein, Biochem. J. 367 (2002) 849–855.
[14] G. Basanez, J.C. Sharpe, J. Galanis, T.B. Brandt, J.M. Hardwick, J. Zimmerberg, Bax-type apoptotic proteins porate pure lipid bilayers through a mechanism sensitive to intrinsic monolayer curvature, J. Biol. Chem. 277 (2002) 49360–49365.
[15] T. Kuwana, M.R. Mackey, G. Perkins, M.H. Ellisman, M. Latterich, R. Schneiter, D.R. Green, D.D. Newmeyer, Bid, Bax, and lipids cooperate to form supramolecular openings in the outer mitochondrial membrane, Cell 111 (2002) 331–342.
[16] O. Terrones, B. Antonsson, H. Yamaguchi, H.G. Wang, J. Liu, R.M. Lee, A. Herrmann, G. Basanez, Lipidic pore formation by the concerted action of proapoptotic BAX and tBID, J. Biol. Chem. 279 (2004) 30081–30091.
[17] J.A. Yethon, R.F. Epand, B. Leber, R.M. Epand, D.W. Andrews, Interaction with a membrane surface triggers a reversible conformational change in Bax normally associated with induction of apoptosis, J. Biol. Chem. 278 (2003) 48935–48941.
[18] E.V. Pavlov, M. Priault, D. Pietkiewicz, E.H. Cheng, B. Antonsson, S. Manon, S.J. Korsmeyer, C.A. Mannella, K.W. Kinnally, A novel, high conductance channel of mitochondria linked to apoptosis in mammalian cells and Bax expression in yeast, J. Cell Biol. 155 (2001) 725–731.
[19] B. Antonsson, S. Montessuit, S. Lauper, R. Eskes, J.C. Martinou, Bax oligomerization is required for channel-forming activity in liposomes and to trigger cytochrome c release from mitochondria, Biochem. J. 345 (Pt 2) (2000) 271–278.
[20] X. Roucou, T. Rostovtseva, S. Montessuit, J.C. Martinou, B. Antonsson, Bid induces cytochrome c-impermeable Bax channels in liposomes, Biochem. J. 363 (2002) 547–552.
[21] R.F. Epand, J.C. Martinou, S. Montessuit, R.M. Epand, Transbilayer lipid diffusion promoted by Bax: implications for apoptosis, Biochemistry 42 (2003) 14576–14582.
[22] R.F. Epand, J.C. Martinou, S. Montessuit, R.M. Epand, C.M. Yip, Direct evidence for membrane pore formation by the apoptotic protein Bax, Biochem. Biophys. Res. Commun. 298 (2002) 744–749.
[23] J.C. Sharpe, D. Arnoult, R.J. Youle, Control of mitochondrial permeability by Bcl-2 family members, Biochim. Biophys. Acta 1644 (2004) 107–113.
[24] S.W. Muchmore, M. Sattler, H. Liang, R.P. Meadows, J.E. Harlan, H.S. Yoon, D. Nettesheim, B.S. Chang, C.B. Thompson, S.L. Wong, S.L. Ng, S.W. Fesik, X-ray and NMR structure of human Bcl-xL, an inhibitor of programmed cell death, Nature 381 (1996) 335–341.
[25] A.M. Petros, A. Medek, D.G. Nettesheim, D.H. Kim, H.S. Yoon, K. Swift, E.D. Matayoshi, T. Oltersdorf, S.W. Fesik, Solution structure of the antiapoptotic protein bcl-2, Proc. Natl. Acad. Sci. U. S. A. 98 (2001) 3012–3017.
[26] A.Y. Denisov, M.S. Madiraju, G. Chen, A. Khadir, P. Beauparlant, G. Attardo, G.C. Shore, K. Gehring, Solution structure of human BCL-w: modulation of ligand binding by the C-terminal helix, J. Biol. Chem. 278 (2003) 21124–21128.
[27] M. Suzuki, R.J. Youle, N. Tjandra, Structure of Bax: coregulation of dimer formation and intracellular localization, Cell 103 (2000) 645–654.
[28] J.M. McDonnell, D. Fushman, C.L. Milliman, S.J. Korsmeyer, D. Cowburn, Solution structure of the proapoptotic molecule BID: a structural basis for apoptotic agonists and antagonists, Cell 96 (1999) 625–634.
[29] J.J. Chou, H. Li, G.S. Salvesen, J. Yuan, G. Wagner, Solution structure of BID, an intracellular amplifier of apoptotic signaling, Cell 96 (1999) 615–624.
[30] J.S. Woo, J.S. Jung, N.C. Ha, J. Shin, K.H. Kim, W. Lee, B.H. Oh, Unique structural features of a BCL-2 family protein CED-9 and biophysical characterization of CED-9/EGL-1 interactions, Cell Death Differ. 10 (2003) 1310–1319.
[31] A.M. Petros, E.T. Olejniczak, S.W. Fesik, Structural biology of the Bcl-2 family of proteins, Biochim. Biophys. Acta 1644 (2004) 83–94.
[32] R. Eskes, S. Desagher, B. Antonsson, J.C. Martinou, Bid induces the oligomerization and insertion of Bax into the outer mitochondrial membrane, Mol. Cell. Biol. 20 (2000) 929–935.
[33] A.J. Garcia-Saez, M. Coraiola, M. Dalla Serra, I. Mingarro, G. Menestrina, J. Salgado, Peptides derived from apoptotic Bax and Bid reproduce the poration activity of the parent full-length proteins, Biophys. J. 88 (2005) 3976–3990.
[34] P.F. Cartron, M. Priault, L. Oliver, K. Meflah, S. Manon, F.M. Vallette, The N-terminal end of Bax contains a mitochondrial-targeting signal, J. Biol. Chem. 278 (2003) 11633–11641.
[35] P.F. Cartron, T. Gallenne, G. Bougras, F. Gautier, F. Manero, P. Vusio, K. Meflah, F.M. Vallette, P. Juin, The first alpha helix of Bax plays a necessary role in its ligand-induced activation by the BH3-only proteins Bid and PUMA, Mol. Cell 16 (2004) 807–818.
[36] P.F. Cartron, H. Arokium, L. Oliver, K. Meflah, S. Manon, F.M. Vallette, Distinct domains control the addressing and the insertion of Bax into mitochondria, J. Biol. Chem. 280 (2005) 10587–10598.
[37] A.J. Garcia-Saez, M. Coraiola, M.D. Serra, I. Mingarro, P. Muller, J. Salgado, Peptides corresponding to helices 5 and 6 of Bax can independently form large lipid pores, FEBS J. 273 (2006) 971–981.
[38] S. Qian, W.C. Wang, L. Yang, H.W. Huang, Structure of transmembrane pore induced by Bax-derived peptide: evidence for lipidic pores, Proc. Natl. Acad. Sci. U. S. A. 105 (2008) 17379–17383.
[39] M.G. Annis, E.L. Soucie, P.J. Dlugosz, J.A. Cruz-Aguado, L.Z. Penn, B. Leber, D.W. Andrews, Bax forms multispanning monomers that oligomerize to permeabilize membranes during apoptosis, EMBO J. 24 (2005) 2096–2103.
[40] Y.T. Hsu, R.J. Youle, Bax in murine thymus is a soluble monomeric protein that displays differential detergent-induced conformations, J. Biol. Chem. 273 (1998) 10777–10783.
[41] A.J. Garcia-Saez, I. Mingarro, E. Perez-Paya, J. Salgado, Membrane-insertion fragments of Bcl-xL, Bax, and Bid, Biochemistry 43 (2004) 10930–10943.
[42] M.A. Sani, C. Loudet, G. Grobner, E.J. Dufourc, Pro-apoptotic bax-alpha1 synthesis and evidence for beta-sheet to alpha-helix conformational change as triggered by negatively charged lipid membranes, J. Pept. Sci. 13 (2007) 100–106.
[43] N. Kucerka, M.P. Nieh, J. Pencer, T.A. Harroun, J. Katsaras, The study of liposomes, lamellae and membranes using neutrons and X-rays, Curr. Opin. Colloid Interface Sci. 12 (2007) 17–22.
[44] J.F. Hunt, P.D. McCrea, G. Zaccai, D.M. Engelman, Assessment of the aggregation state of integral membrane proteins in reconstituted phospholipid vesicles using small angle neutron scattering, J. Mol. Biol. 273 (1997) 1004–1019.
[45] Z. Bu, L. Wang, D.A. Kendall, Nucleotide binding induces changes in the oligomeric state and conformation of Sec A in a lipid environment: a small-angle neutron-scattering study, J. Mol. Biol. 332 (2003) 23–30.
[46] R.J. Gilbert, R.K. Heenan, P.A. Timmins, N.A. Gingles, T.J. Mitchell, A.J. Rowe, J. Rossjohn, M.W. Parker, P.W. Andrew, O. Byron, Studies on the structure and mechanism of a bacterial protein toxin by analytical ultracentrifugation and small-angle neutron scattering, J. Mol. Biol. 293 (1999) 1145–1160.
[47] H.B. Bosmann, A. Hagopian, E.H. Eylar, Cellular membranes: the isolation and characterization of the plasma and smooth membranes of HeLa cells, Arch. Biochem. Biophys. 128 (1968) 51–69.
[48] J.F. Nagle, S. Tristram-Nagle, Structure of lipid bilayers, Biochim. Biophys. Acta 1469 (2000) 159–195.
[49] J. Zha, S. Weiler, K.J. Oh, M.C. Wei, S.J. Korsmeyer, Posttranslational N-myristoylation of BID as a molecular switch for targeting mitochondria and apoptosis, Science 290 (2000) 1761–1765.
[50] J.F. Lovell, L.P. Billen, S. Bindner, A. Shamas-Din, C. Fradin, B. Leber, D.W. Andrews, Membrane binding by tBid initiates an ordered series of events culminating in membrane permeabilization by Bax, Cell 135 (2008) 1074–1084.

[51] Y.T. Hsu, R.J. Youle, Nonionic detergents induce dimerization among members of the Bcl-2 family, J. Biol. Chem. 272 (1997) 13829–13834.
[52] M. Abramoff, P. Magelhaes, S. Ram, Image processing with ImageJ, Biophotonics Int. 11 (2004) 36–42.
[53] D. Satsoura, B. Leber, D.W. Andrews, C. Fradin, Circumvention of fluorophore photobleaching in fluorescence fluctuation experiments: a beam scanning approach, Chemphyschem 8 (2007) 834–848.
[54] A. Abu-Arish, A. Porcher, A. Czerwonka, N. Dostatni, C. Fradin, High mobility of bicoid captured by fluorescence correlation spectroscopy: implication for the rapid establishment of its gradient, Biophys. J. 99 (2010) L33–L35.
[55] M. Wachsmuth, W. Waldeck, J. Langowski, Anomalous diffusion of fluorescent probes inside living cell nuclei investigated by spatially-resolved fluorescence correlation spectroscopy, J. Mol. Biol. 298 (2000) 677–689.
[56] P. Kask, K. Palo, D. Ullmann, K. Gall, Fluorescence-intensity distribution analysis and its application in biomolecular detection technology, Proc. Natl. Acad. Sci. U. S. A. 96 (1999) 13756–13761.
[57] N. Ben-Tal, B. Honig, R.M. Peitzsch, G. Denisov, S. McLaughlin, Binding of small basic peptides to membranes containing acidic lipids: theoretical models and experimental results, Biophys. J. 71 (1996) 561–575.
[58] E. Grant Jr., T.J. Beeler, K.M. Taylor, K. Gable, M.A. Roseman, Mechanism of magainin 2a induced permeabilization of phospholipid vesicles, Biochemistry 31 (1992) 9912–9918.
[59] C.J. Glinka, J.G. Barker, B. Hammouda, S. Krueger, J.J. Moyer, W.J. Orts, The 30m small-angle neutron scattering instruments at the National Institute of Standards and Technology, J. Appl. Crystallogr. 31 (1998) 430–445.
[60] S.R. Kline, Reduction and analysis of SANS and USANS data using IGOR Pro, J. Appl. Crystallogr. 39 (2006) 895–900.
[61] N. Kučerka, J.F. Nagle, S.E. Feller, P. Balgavý, Models to analyze small-angle neutron scattering from unilamellar lipid vesicles, Phys. Rev. E 69 (2004) 051903–051912.
[62] J. Pencer, S. Krueger, C.P. Adams, J. Katsaras, Method of separated form factors for polydisperse vesicles, J. Appl. Crystallogr. 39 (2006) 293–303.
[63] N. Kucerka, J. Pencer, J.N. Sachs, J.F. Nagle, J. Katsaras, Curvature effect on the structure of phospholipid bilayers, Langmuir 23 (2007) 1292–1299.
[64] L. Yu, M. Tan, B. Ho, J.L. Ding, T. Wohland, Determination of critical micelle concentrations and aggregation numbers by fluorescence correlation spectroscopy: aggregation of a lipopolysaccharide, Anal. Chim. Acta 556 (2006) 216–225.
[65] Svergun Feigin, Structure Analysis by Small Angle X-Ray and Neutron Scattering, Plenum Press, New York, 1987.
[66] Lucken-Ardjomande, Cell Death Differ. 15 (2008) 929.
[67] G. Kudla, S. Montessuit, R. Eskes, C. Berrier, J.C. Martinou, A. Ghazi, B. Antonsson, The destabilization of lipid membranes induced by the C-terminal fragment of caspase 8-cleaved bid is inhibited by the N-terminal fragment, J. Biol. Chem. 275 (2000) 22713–22718.
[68] G. Basanez, A. Nechushtan, O. Drozhinin, A. Chanturiya, E. Choe, S. Tutt, K.A. Wood, Y. Hsu, J. Zimmerberg, R.J. Youle, Bax, but not Bcl-xL, decreases the lifetime of planar phospholipid bilayer membranes at subnanomolar concentrations, Proc. Natl. Acad. Sci. U. S. A. 96 (1999) 5492–5497.
[69] M. Karbowski, K.L. Norris, M.M. Cleland, S.Y. Jeong, R.J. Youle, Role of Bax and Bak in mitochondrial morphogenesis, Nature 443 (2006) 658–662.
[70] B. Westermann, Molecular machinery of mitochondrial fusion and fission, J. Biol. Chem. 283 (2008) 13501–13505.
[71] C.M. Franzin, J. Choi, D. Zhai, J.C. Reed, F.M. Marassi, Structural studies of apoptosis and ion transport regulatory proteins in membranes, Magn. Reson. Chem. 42 (2004) 172–179.
[72] S.D. Zakharov, W.A. Cramer, Insertion intermediates of pore-forming colicins in membrane two-dimensional space, Biochimie 84 (2002) 465–475.
[73] X.M. Gong, J. Choi, C.M. Franzin, D. Zhai, J.C. Reed, F.M. Marassi, Conformation of membrane-associated proapoptotic tBid, J. Biol. Chem. 279 (2004) 28954–28960.
[74] K.J. Oh, S. Barbuto, N. Meyer, R.S. Kim, R.J. Collier, S.J. Korsmeyer, Conformational changes in BID, a pro-apoptotic BCL-2 family member, upon membrane binding. A site-directed spin labeling study, J. Biol. Chem. 280 (2005) 753–767.
[75] V.G. Veresov, A.I. Davidovskii, Monte Carlo simulations of tBid association with the mitochondrial outer membrane, Eur. Biophys. J. 37 (2007) 19–33.
[76] L. Song, M.R. Hobaugh, C. Shustak, S. Cheley, H. Bayley, J.E. Gouaux, Structure of staphylococcal alpha-hemolysin, a heptameric transmembrane pore, Science 274 (1996) 1859–1866.
[77] F. Edlich, S. Banerjee, M. Suzuki, M.M. Cleland, D. Arnoult, C.X. Wang, A. Neutzner, N. Tjandra, R.J. Youle, Bcl-x(L) Retrotranslocates Bax from the Mitochondria into the Cytosol, Cell 145 (2011) 104–116.
[78] V.G. Veresov, A.I. Davidovskii, Activation of Bax by joint action of tBid and mitochondrial outer membrane: Monte Carlo simulations, Eur. Biophys. J. 38 (2009) 941–960.
[79] E. Gouaux, Channel-forming toxins: tales of transformation, Curr. Opin. Struct. Biol. 7 (1997) 566–573.
[80] H.W. Huang, Molecular mechanism of antimicrobial peptides: the origin of cooperativity, Biochim. Biophys. Acta 1758 (2006) 1292–1302.
[81] M.-T. Lee, W.-C. Hung, F.-Y. Chen, H.W. Huang, Mechanism and kinetics of pore formation in membranes by water-soluble amphipathic peptides, Proc. Natl. Acad. Sci. U. S. A. 105 (2008) 5087–5092.
[82] M.L. Longo, A.J. Waring, L.M. Gordon, D.A. Hammer, Area expansion and permeation of phospholipid membrane bilayers by influenza fusion peptides and melittin, Langmuir 14 (1998) 2385–2395.
[83] H.W. Huang, F.Y. Chen, M.T. Lee, Molecular mechanism of peptide-induced pores in membranes, Phys. Rev. Lett. 92 (2004) 198304.
[84] H.W. Huang, Free energies of molecular bound states in lipid bilayers: lethal concentrations of antimicrobial peptides, Biophys. J. 96 (2009) 3263–3272.
[85] T. Ursell, K.C. Huang, E. Peterson, R. Phillips, Cooperative gating and spatial organization of membrane proteins through elastic interactions, PLoS Comput. Biol. 3 (2007) e81.
[86] B.J. Reynwar, G. Illya, V.A. Harmandaris, M.M. Muller, K. Kremer, M. Deserno, Aggregation and vesiculation of membrane proteins by curvature-mediated interactions, Nature 447 (2007) 461–464.
[87] C. Tan, P.J. Dlugosz, J. Peng, Z. Zhang, S.M. Lapolla, S.M. Plafker, D.W. Andrews, J. Lin, Auto-activation of the apoptosis protein Bax increases mitochondrial membrane permeability and is inhibited by Bcl-2, J. Biol. Chem. 281 (2006) 14764–14775.
[88] A.J. Garcia-Saez, J. Ries, M. Orzaez, E. Perez-Paya, P. Schwille, Membrane promotes tBID interaction with BCL(XL), Nat. Struct. Mol. Biol. 16 (2009) 1178–1185.
[89] G. Fuertes, D. Gimenez, S. Esteban-Martin, A. Garcia-Saez, O. Sanchez, J. Salgado, Role of membrane lipids for the activity of pore forming peptides and proteins, Adv. Exp. Med. Biol. 677 (2010) 31–55.